

Università degli Studi di Napoli “Federico II”



Centro Interdipartimentale di Ricerca Ambiente  
C.I.R.AM.

Dottorato di ricerca in  
ANALISI DEI SISTEMI AMBIENTALI

XXVI CICLO

SETTORE SCIENTIFICO DISCIPLINARE GEO/11- GEOFISICA APPLICATA

PhD Thesis

# **Imaging of Potential Fields for Mining and Environmental Applications**

*Mahmoud Ahmed Abbas Ahmed*

**Tutor:**

Prof. Maurizio Fedi

**PhD Coordinator:**

Prof. Maurizio Fedi

Academic year 2014/2015

*To my parents, my wife and my daughter.*

## *Contents*

Summary .....	4
Introduction .....	7
Chapter 1	
Interpretation of self-potential data using the DEXP method.	
1.1 Introduction .....	10
1.2 Theory.....	12
1.3 Determining the depth to the source by the geometrical method .....	18
1.4 Determining the scaling law: estimation of the scaling exponent .....	19
1.5 Synthetic Examples .....	20
1.6 Field Examples .....	26
Chapter 2	
Application of the DEXP method to the streaming potential data.	
2.1 Introduction .....	32
2.2 Theory .....	33
2.3 Synthetic Example .....	36
2.4 Real Examples .....	38
Chapter 3	
Automatic DEXP Imaging of Potential Fields Independent of the Structural Index.	
3.1 Introduction .....	44
3.2 Theory .....	45
3.3 Estimation of the Structural Index .....	51
3.4 Noise and non-linear effects .....	53
3.5 Field Examples .....	56
Chapter 4	
Improving the local wavenumber method by automatic DEXP transformation.	
4.1 Introduction .....	61
4.2 Theory .....	62
4.3 Synthetic Examples .....	65
4.4 Field Examples .....	70
Chapter 5	
Fractional-order local wavenumber: an improved source-parameter estimator.	
5.1 Introduction .....	74
5.2 Theory .....	74

5.3 Synthetic Examples .....	77
5.4 Field Examples .....	80
Conclusions .....	83
Appendices	
A. Division by zero problem in the automatic DEXP method.....	87
B. The homogeneity-degree of the ratio of potential fields of different orders and the ridge behaviour .....	89
C. Numerical evaluation of the $N$ -dependent local-wavenumber equation by Smith et al. (1998) for a fractional order.....	90
References .....	91
Acknowledgements .....	103

## *Summary*

In this thesis I tried to develop new automatic imaging methods, aiming at improving the interpretation of potential field anomalies related to mining and environmental studies. The major improvements, which I obtained, are the stability, which is normally low for methods such as the local wavenumber, and the full automaticity in retrieving the source parameters (depth and structural index).

Starting from the theory of the Depth from Extreme Points (DEXP) method, I first applied it to the self-potential data related to mineralization and to groundwater flow. DEXP is a fast imaging method transforming the field data, or its derivatives, into a quantity proportional to the source distribution. The method is particularly suited to handle at high-resolution noisy data, as it is stable even using high-order derivatives. DEXP imaging depends on the knowledge of the structural index of the source. While this parameter may be a priori determined by the method itself, i.e., by a preliminary application of related multiscale methods based on the study of the scaling function, it may also assumed a priori, as done for other imaging methods such as migration, correlation or the sandwich model. I showed the usefulness of DEXP method to self-potential datasets, regarding mineral exploration at Malachite mine, Colorado, (USA), Sariyer area (Turkey) and Bender area (India) and water-table depth estimation in a pumping well and in sinkholes at the area of San Vittorino Plain (Rieti, central Italy). The estimated depths well agree with the known information about the sources.

As any imaging method (DEXP, correlation, migration and others) needs to assume, inherently or explicitly, a value for the structural index and that it is valid throughout the whole explored source volume, I tried to develop new imaging methods to estimate the depth to the sources of potential fields independent from value of the structural index. The first of them consists of applying the DEXP transformation to the ratio ( $\mathcal{R}$ ) between two different-

order partial derivatives of the field. While the scaling function used in the DEXP transformation depends on the structural index, I showed that the scaling function of  $\mathcal{H}$  merely depends on the difference between the two used orders of differentiation. This allows three main features to be established for the DEXP transformation of  $\mathcal{H}$ : a) it is independent from the structural index; b) the estimation of the source depths is fully automatic, simply consisting in the search of position of the extreme points of the DEXP image; c) the structural index of each source is finally determined from the scaling function or the extreme points using the estimated depth. Besides the well known characteristics of the DEXP transformation, such as high-resolution and stability, the DEXP transformation of  $\mathcal{H}$  enjoys one more relevant feature: it can be applied to multi-source cases, yielding simultaneously correct estimations of structural index and depth for each source in the same image. However, while the DEXP transformation is a linear transformation of the field, the DEXP transformation of  $\mathcal{H}$  is nonlinear, and a procedure is described to circumvent the nonlinear effects.

The method is tested with synthetic examples and applied to real magnetic data for mineral exploration from the Pima copper mine, Arizona, USA, Hamrawien area, Egypt and Cataldere, Bala district of Turkey. The results are consistent with the known information about the causative sources.

I developed also a method for source parameter estimation, based on the local wavenumber function. Even in this case I made use of the stable properties of the DEXP method, so to deal with local wavenumber of high-order, as DEXP is able to overcome its known instability caused by the use of high-order derivatives. Also in this case, i.e., the DEXP transformation of the local wavenumber, the scaling-law is independent of the structural index, is fully automatic and may be implemented as a very fast imaging method, mapping different-kind sources at their own correct depth. The method was demonstrated to

synthetic cases and applied to real-data examples from Bulgaria and from a test site for buried drums in Italy.

I also developed a new method to analyze the local wavenumber, based on the fractional-order differentiation of potential fields, to the end of applying it in a more stable way. Such kind of differentiation allows a fractional-order local wavenumber to be defined, whose usefulness is two-fold: a) the positions of the peaks of the two different-order local wavenumber are essentially the same; b) the well known instability of the method, due to the noise-enhancement related to the field standard differentiation, may be kept to a minimum, if a fractional-order field differentiation is used. The method is applied to synthetic and real examples for mineralization and archaeological exploration and it provided a good estimation of both depth to sources and structural index.

## ***Introduction***

Gravity and magnetics are examples of passive geophysical methods. The non-invasive surveys of magnetic and gravimetric fields have the ability to provide information in relatively short time and low cost, even over large areas.

Gravity method is a potential field technique, which involves measurements of the spatial variations in the Earth's gravitational field. These variations are caused by density contrasts in the Earth's rocks. It has many geological and environmental applications such as regional geological mapping; oil and gas exploration, sediment thickness studies, mineral exploration, archaeological surveys, and cavity detection for urban applications.

Magnetic method is another passive method related to measurements of the variations in the geomagnetic field. Such measurements are the sum of different contributions: the main field, produced in the fluid core by means of a mechanism that goes under the name of geodynamo; the crustal field, produced by the magnetized rocks of the terrestrial crust. The typical applications of the magnetic method are in the fields of archaeology, mineral exploration, and geological and environmental mapping (e.g., the search of buried ferromagnetic objects).

The self-potential method is one of the oldest geophysical methods; it involves measurements of the natural electric potential on the Earth's surface with two potential electrodes. The self-potential anomalies have a mathematical form similar to that of the gravity and magnetic field. For this reason, the interpretation methods of potential field methods can also be applied to the self-potential data. The interpretation of self-potential data for the monitoring of environmental problems such as detection of mineralization, water table, cavities and sinkholes, geothermal power and contamination is appreciated in geophysical literature.

The interpretation methods are greatly improved with the development of automatic modelling programs and by introducing new analysis methods, not only in order to locate the position of the sources, but also to determine the shape and physical property. One category of these methods is that of multiscale methods such as the Depth from EXtreme Points (DEXP) method (Fedi, 2007), in which the field at different levels or altitudes is scaled with a scaling-law. The form of the scaling law theoretically depends on the structural index  $N$ , a quantity related to the geometry of the source. So the method involves an a priori estimation of  $N$ . However, it may be fixed arbitrarily, similar to other imaging methods (migration, for instance, which intrinsically assume cylinder-like sources (Fedi and Pilkington, 2012, Table 2). The scaled field at different altitudes yields an image of the source distribution where the extreme points indicate the depth to the source. The method is fast, accurate and stable against noise and at whatever-order differentiation of the field.

The first goal of this thesis is to introduce the application of the DEXP method in the interpretation of self-potential data, related to mineral exploration and environmental studies of ground water flow such as well-pumping monitoring and sinkholes detection.

The second goal is to develop an automatic DEXP imaging method independent from the value of the structural index of the causative source and apply it to examples for mineral exploration.

The third goal is making use of the stable properties of the DEXP method to improve the local-wavenumber method for the estimation of the depth and shape of the causative sources and apply this new imaging approach to real examples for mineral exploration and finding of buried metal drums.

The fourth goal is to introduce a fractional-order local wavenumber to attenuate the effect of noise in the data, to improve the estimation of depth and shape of the causative sources and to apply this new approach to examples of archaeology and mineral exploration.

The software codes written during this thesis are:

- MATLAB<sup>TM</sup> codes of 2D and 3D *AUTOMATIC DEXP* applied to the ratio between two derivatives of the field.
- MATLAB<sup>TM</sup> codes of 2D and 3D *AUTOMATIC DEXP* applied to two analytic signal moduli of the field.
- MATLAB<sup>TM</sup> codes of 2D and 3D *LOCAL-WAVENUMBER DEXP* imaging.
- MATLAB<sup>TM</sup> code for calculating the *FRACTIONAL-ORDER LOCAL WAVENUMBER* and estimation of depth and structural index of the causative sources.

By the end of my doctorate three articles from this thesis are already published in peer-reviewed international journals:

- Fedi, M., and Abbas, M. A., 2013, A fast interpretation of self-potential data using the depth from extreme points method. *Geophysics*, 78(2), E107-E116.
- Abbas, M. A., and Fedi, M. (2014). Automatic DEXP imaging of potential fields independent of the structural index. *Geophysical Journal International*, 199(3), 1625-1632.
- Abbas, M. A., Fedi, M., and Florio, G., 2014, Improving the local wavenumber method by automatic DEXP transformation. *Journal of Applied Geophysics*, 111, 250-255.

Two other articles are just to be submitted to peer-reviewed international journals.

# ***Chapter 1***

## ***Interpretation of self-potential data using the DEXP method***

*This chapter is published as:* Fedi, M., and Abbas, M. A., 2013, A fast interpretation of self-potential data using the depth from extreme points method. *Geophysics*, 78(2), E107-E116.

### **1.1 Introduction**

Self-potential method (SP) is one of the oldest geophysical methods. It involves measurements of ground electric potential, as developed in the Earth by many source mechanisms. An often-referenced mechanism for explaining the self-potential, even if not so general, is due to Sato and Mooney (1960). It requires the causative body to straddle the water table; below it, electrolytes in the pore fluids undergo oxidation and release electrons, which are conducted upwards through the ore body. At the top of the body, the released electrons cause reduction of the electrolytes. A circuit thus exists, in which current is carried electrolytically in the pore fluids and electronically in the body, so that the top of the body acts as a negative terminal.

Many methods of interpretation were developed for self-potential data. They include methods assuming a fixed-geometry for the sources (e.g., Yüngül, 1950; Meiser, 1962; Paul, 1965; Bhattacharya and Roy, 1981, Rao and Babu, 1983), methods using Fourier analysis (e.g., Rao et al., 1982), and inverse methods (e.g., Shi and Morgan, 1996, Jardani et al., 2007; Minsley et al., 2007 and Mendonça, 2008). Assuming a simple geometry for the sources requires a prior knowledge of the shape of the anomalous body and most of the methods use few characteristic points and distances, nomograms, or standardised curves to determine the depth. Thus, they are highly subjective and can lead to major errors in estimating the depth of the buried structure. On the other hand inverse methods are computationally expensive.

Other methods are based on the continuous wavelet transform (CWT), which allows the characterization of discontinuities or abrupt changes in the measured signal. For potential fields the Poisson kernel family is normally used (e.g., Moreau et al., 1997, Sailhac and Marquis, 2001, Fedi et al., 2010); a recent extension of the CWT applied to potential fields allows the use of any kind of wavelet (Fedi and Cascone, 2011). Depths are determined at the intersection of the maxima of the absolute values of the field lines (amplitude of the wavelet coefficient), which converge to the source. In the wavelet transform method the type of the source is not assumed but is derived by a direct estimation of the structural index from the CWT coefficients. Gilbert and Sailhac (2008) noted, however, that the CWT is not simply related to the source distribution, so it cannot be easily used as an imaging method.

SP anomalies have also been interpreted through cross-correlation of the field with that by assumed elementary scanning-sources, for example a point-source by Patella (1997a, b) and a dipole-source by Revil et al. (2001) and Iuliano et al. (2002). The zero-lag cross-correlation may be mapped at different depths and horizontal positions of the scanning-source, so describing a possible distribution of source density, this depending however on the a priori type of scanning-source used, e.g. a single pole, a dipole or any other. The correlation method has an inherent lack of criteria to assess a priori the best type of scanning-source (Gilbert and Sailhac, 2008). In fact Bhattacharya et al. (2007) compared the cross-correlation results for dipole and pole sources of SP data over graphite and sulphide ore deposits in India, but were not able to indicate the best result.

The enhanced local wave-number technique (Salem et al., 2005) was applied by Srivastava and Agarwal (2009) to the interpretation of the SP anomalies. The basic advantage of this technique lies with the determination of the location and depth without a priori knowledge of the nature of the causative source. In fact, the structural index is obtained from the earlier determined parameters. The drawback of this technique is that it is sensitive to

noise, due to second-order derivatives computation. Recently, Agarwal and Srivastava (2009) applied the conventional and extended Euler homogeneity equation (Thompson, 1982; and Mushayandebvu et al., 2001) to analyze self-potential anomalies and so compute the location, depth and the structural index of the causative source.

Fedi (2007) introduced the Depth from Extreme Points method (DEXP) to estimate the depth to the causative source, the excess mass or the dipole moment intensity and the structural index from potential field data. The first two source parameters are estimated by the extreme points values of the DEXP transformed field; the structural index, a parameter related to the kind of the source, may be estimated in several ways, for example from the invariance of the estimated depth with respect to the order of the DEXP transformation and from the evaluation of the scaling exponent intercept. The method has a very low sensitivity to noise and, differently from CWT, it is also an imaging method, providing a meaningful image of the source distribution (Fedi et al., 2010; Fedi and Pilkington, 2012). Here, we adapt the DEXP transformation to the interpretation of SP anomalies, in order to estimate the horizontal location, the depth and the structural index of the sources.

## **1.2 Theory**

There are two major contributions to the self-potential anomaly: the reduction-oxidation effect, associated with ore bodies and organic matter-rich-contaminants, and the streaming potential, related to water flow. Other contributions, like diffusion potential and thermo-electrical effects, have minor relevance (Jardani et al. 2008). Also, the effect of the reduction-oxidation and streaming potential can be separated (see Trique et al., 2002; Naudet et al., 2003; 2004; Rizzo et al., 2004). According to Patella (1997), despite of the many possible source models, SP anomalies are the surface evidence of a (approximately) steady state of electric polarization, related to electric circulation in conductive rocks. Hence, the

inverse SP problem consists of finding the location and the geometries of any accumulated electric charge underground.

In this chapter, we will use the DEXP theory to interpret the SP anomalies of interest for mineral exploration. In such cases, we mainly expect that SP anomalies are produced by reduction-oxidation processes of mineralization, in the form of electrically polarized bodies within a homogeneous subsurface. In this case, the simplest SP anomalies are produced, due to the accumulation of positive and negative charges in the form of either compact point poles (for spherical target) or pole lines (for cylindrical and sheet type targets). Thus, point poles and lines of poles may be considered as fundamental blocks for obtaining the SP anomalies due to more complicated pattern of positive and negative poles distributed in 3-D space (Agarwal, 1984).

The total SP anomaly can be defined as:

$$S(P) = \int_V \nabla \cdot \frac{\mathbf{K}}{r} dv \quad (1-1)$$

where  $\mathbf{K}$  is the electric dipole moment due to charge accumulation, either primary or induced, and  $r$  is the distance from the observation point  $P$ .

From a mathematical point of view, the theory of self-potential anomalies is quite similar to that for gravity and magnetic prospecting. For instance, the electric field and the electric potential due to a body with uniform polarization are analogous to the magnetic field and the magnetic scalar potential associated with the body, whenever it is uniformly magnetized in the same direction as the electric polarization. Hence, the electric potential has the same mathematical form as the magnetic potential and, in case of vertical polarization, as the gravity field (Babu, 2003).

As stated above, DEXP is a high resolution, stable method for estimating the source depth and structural index. The DEXP transformation is carried out by scaling a potential field

according to scaling laws of different form, related to the structural index or, in other words, to the model-type of the source (such as poles, dipoles or others). The important point is that the structural index may be experimentally determined from the measured data themselves. Alternatively one may simply assume a given source-model. Once the structural index is determined, the second step is to transform the field by scaling it with an appropriate scaling law. The depths to sources are then obtained from the extreme points of the transformed field.

We here outline briefly the theory of the DEXP method in the case of the SP. For further details, refer to Fedi (2007), in which the whole theory for potential fields is detailed. Let us consider any  $p^{th}$  order directional derivative of a homogeneous Newtonian potential  $U$ :

$$f_p = \frac{\partial^p U(z)}{\partial z^p} \quad (1-2)$$

A key concept in the DEXP theory is the scaling function  $\tau_p$ . According to Fedi (2007)  $\tau_p$  may be defined as the derivative of the logarithm of the  $p^{th}$  derivative  $f_p(z)$  of  $U$  with respect to  $\log(z)$ :

$$\tau_p = \frac{\partial \log f_p(z)}{\partial \log(z)} = -(p+1) \frac{z}{z-z_0} \quad (1-3)$$

where  $-(p+1)$  is the homogeneity degree of  $f_p$ ,  $z$  is the altitude and  $z_0$  is the depth to the source. As said before, the elementary sources involved in the SP method are of dipolar nature. From a mathematical point of view, we may therefore refer to the DEXP theory of the magnetic potential (Fedi, 2007). So, for the SP of a dipole source (or a polarized sphere) we may pose  $p=1$  and  $S=f_1$  in equation (1-3). The scaling function of  $S$  at  $x_0=y_0=0$ , then becomes

$$\tau = \frac{\partial \log S}{\partial \log(z)} = \frac{-2z}{z-z_0} \quad (1-4)$$

Note that  $\tau$  is singular in the source region, at  $z=z_0$ . The most interesting thing, however, is that in the harmonic region, at  $z=-z_0$ :

$$\tau = \frac{\partial \log S}{\partial \log(z)} = -1, \quad (1-5)$$

According to Fedi (2007) we deduce from equation (1-5) that:

$$\frac{\partial \log S}{\partial z} = - \frac{\partial \log(z)}{\partial z} \quad (1-6)$$

or:

$$\frac{\partial [\log S + \log(z)]}{\partial z} = 0 \quad (1-7)$$

which means that:

$$\frac{\partial (zS)}{\partial z} = 0 \quad (1-8)$$

From equation (1-8) it is now easy to argue that the function  $\Omega$  formed by scaling the SP,  $S$  with the power law  $z$

$$\Omega = zS \quad (1-9)$$

has its extreme point (a maximum or a minimum) at  $z=-z_0$ . The scaled field  $\Omega$  is called the DEXP function. This result generalizes for any  $p$ -order derivative of the SP, for which the scaling function writes:

$$\tau_p = \frac{-(p+2)z}{z-z_0} \quad (1-10)$$

where  $-(p+2)$  is the homogeneity degree of the  $p$ -order derivative of the SP.

The structural index  $N_p$ , a quantity associated to the shape of the source in the Euler deconvolution theory (Thompson, 1982), has been defined as the opposite of the homogeneity degree for the magnetic field or for the gravity field. We can rewrite equation (1-10) as:

$$\tau_p = \frac{-N_p z}{z-z_0} \quad (1-11)$$

If we let  $N$  to indicate the structural index in the case of the self-potential,  $N_I$  will refer to that of its first-order derivative (or its electric field) and so on. This is similar to the gravity method where  $N$  refers to the gravity field and  $N_I$  refers to its first-order derivative. In the SP method,  $N$  assumes the values [2, 1, 0, -1] respectively for the polarized sphere (3D), the horizontal cylinder (2D), the dyke (2D) and the contact (2D) (see Table 1.1). According to Fedi (2007),  $N_p$  will be given simply by:

$$N_p = p + N. \quad (1-12)$$

Hence the DEXP transformation is generalized as:

$$\Omega_p(z) = z^{N_p/2} f_p(z), \quad (1-13)$$

where  $z$  is any altitude greater or equal to the measurement level  $z_m$ .

Scaling properties of sources have been derived from power spectra of potential fields for fractal modelling of density and magnetic susceptibility (Pilkington and Todoeschuck, 1993; Fedi, 2003; Bansal and Dimri, 2005; Bansal et al., 2010). For homogeneous functions, the scaling law in equation (1-13) is also related to the source-distribution homogeneity. Note however that, differently from power spectrum estimates of depth, which are only localized in frequency, the DEXP transformation estimates are localized in both space and scale (altitude), which is in turn related to frequency.

Table 1.1: Source-types and related structural indices for the SP and its first- and second-order derivatives.

Source model	Depth to	$N$ (SP)	$N_1$ (first-order derivative of SP)	$N_2$ (second order derivative of SP)
Dipoles, Spheres	center	2	3	4
Line of dipoles, infinite horizontal or vertical cylinder, thin bottomless prism, point-pole	Center or top	1	2	3
Semi-infinite plane, thin dyke, sill	Center or top	0	1	2
Semi-infinite contact	top	-1	0	1

We argue from equation (1-13) that, in order to scale the field and form the DEXP function, we must either assume or estimate the structural index (equation 1-12). The structural index  $N_p$  may be estimated from the scaling function in several ways (see Fedi and Florio, 2006; Fedi, 2007). To this end, we will describe in the next section the most suitable approach. From equation (1-13), it is clear that the numerical implementation of the method uses upward continuation and vertical differentiation of order  $p$  for the computation of  $f_p$  and  $\tau_p$ . At a first sight, upward continuation should not be allowed for SP anomalies, being the air

infinitely resistive. A similar problem also occurs for Euler Deconvolution and enhanced local wavenumber methods applied to SP data, where the vertical derivative of the field is also needed (Agarwal and Srivastava, 2009; Srivastava and Agarwal, 2009). We nevertheless agree with those authors that the upward continuation of SP, from the measurement level  $z_m$  to the level  $z_m+a$ , is physically consistent. In fact it may be viewed as the SP at  $z_m$  of the same source located not at  $z_0$  but at the deeper depth  $z_0+a$ . The meaning of the vertical derivative follows consequently.

In conclusion, the DEXP transformation of the SP and of its derivatives is a full 3D method, enjoying important properties: a) its maxima (and minima) correspond to the depth to the source; b) the scaling function analysis allows the structural index (and so the shape of the source) to be estimated as well. In other words, no a priori assumptions about the kind of elementary source are necessary. This property does not hold in the correlation method (Patella, 1997a, 1997b) in which the concept of charge occurrence probability (COP) was introduced through the cross-correlation of the field with that of a point-source, assumed a priori. Similar considerations apply also to the so-called dipole occurrence probability (DOP), defined as the cross-correlation of the field with that of a dipole-source, once again assumed a priori and not estimated by the data (Revil et al., 2001).

One more main property of the DEXP is its high stability, with respect to the noise level and to the differentiation order of the potential. This was shown in several papers (Fedi, 2007; Cella et al., 2009 and others) as due to the optimal mixing, in a single operator, of the wavenumber low-pass behaviour of the upward continuation operator with the enhancement high-pass properties of a  $p$ -order derivative operator. In practice, the behaviour of the DEXP operator in the frequency domain was shown to be that of a band-pass filter, even when a high-order differentiation of the original signal is involved. This performance makes the DEXP transformation a high-resolution imaging method. We note, finally, that the DEXP

transformation, in the case of multi-sources, allows analysis of sources at different depths with no filtering pre-separation (Fedi, 2007).

### **1.3 Determining the depth to the source by the geometrical method**

As a consequence of the dilation of potential fields versus the altitude, the maxima of the field modulus describe lines across the altitudes (ridges). These lines are defined by the zeros of the horizontal and vertical derivatives of the potential field at all the continued levels, forming a so-called multiridge set (Fedi et al., 2009). The number of ridges depends on the order of partial differentiation of the SP data. Moreau et al., (1997) first noted that these lines may be easily extrapolated in the source region, where we can estimate the position of the sources at their intersection (the centre of a sphere, the top of a dyke, etc.). This method has been called the “geometrical method” by Fedi et al., (2009), who extended it to the multiridge set and linked it to the DEXP theory. Figure 1.1 shows the SP anomaly of a point pole of unit strength at a position  $[x_0, y_0, z_0]=[0, 0, 10]$  m together with its second-order vertical derivative. The ridges computed for the second vertical derivative of the self-potential are shown (solid cyan lines). We considered the second-order vertical derivative in order to obtain a consistent number of ridges. We recall that the number of ridges increases with the order of differentiation (Fedi et al., 2009). Note how the ridges intersect each other at the right source position.

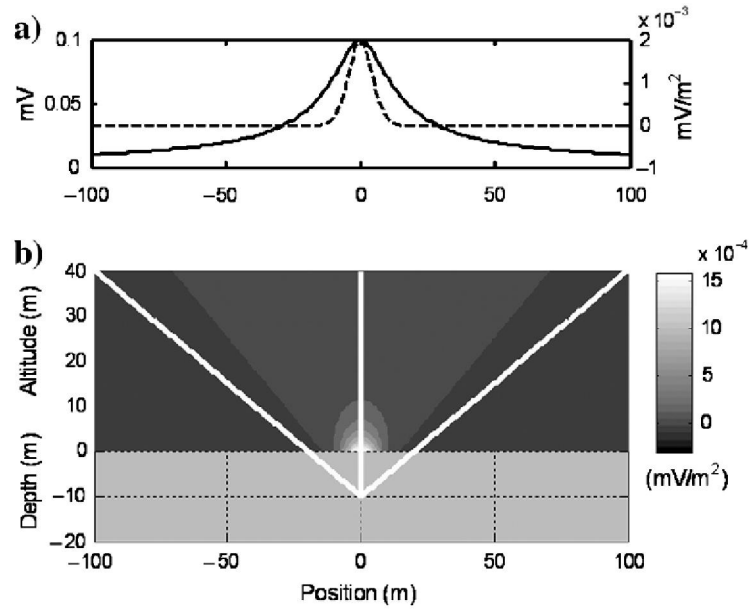


Figure 1.1: Estimation of the depth to the source by the geometrical method.(a) The SP (solid line) and its second vertical derivative (dashed line) of a unit-strength point pole at 10 m and (b) ridges (white solid lines) for the second vertical derivative of the potential of the point pole. Note that the ridges intersect at the right source position.

#### 1.4 Determining the scaling law: estimation of the scaling exponent

We saw previously that the DEXP transformation needs the scaling law  $z^{N_p/2}$  to be fixed, to be effective. The structural index  $N_p$  may be either assumed or estimated from the data before performing DEXP. This task may be easily fulfilled by analyzing the scaling function along any ridge, because it contains all the necessary information.

Noting that the altimetry zero-level is arbitrary, the altitude and depth may be shifted by a guess quantity  $\dot{z}_0$  as  $z - \dot{z}_0$  and  $z_0 - \dot{z}_0$ , respectively. Hence, updating equation (1-11) in such way and putting  $z=l/q$ , we obtain that, for any given guess  $\dot{z}_0$ , the corresponding scaling function assumes the form:

$$\tau_p(q, \dot{z}_0) = -\frac{N_p(1-\dot{z}_0q)}{1-z_0q}. \quad (1-14)$$

This means that, depending on the guess depth  $\dot{z}_0$ ,  $\tau_p$  will be a decreasing, increasing or constant function of  $q$ , respectively for  $\dot{z}_0$  lower, greater or equal to the true  $z_0$ . The structural index  $N_p$  is given with a good accuracy by the intercept of  $\tau_p$  versus  $q$ , provided  $\dot{z}_0$  is reasonably not too far from the true depth to the source (Fedi and Florio, 2006). Note also that the depth  $z_0$  can be estimated by the guess  $\dot{z}_0$  yielding the best approximation to a zero-slope for  $\tau_p$  (Florio et al., 2009). As an example, we select the vertical ridge of the 2<sup>nd</sup> order vertical derivative on Figure (1.1b) and compute the corresponding scaling function by using equation (1-11). We obtain  $N_2=3$ , corresponding to  $N=1$  in the case of potential, according to equation (1-12), (Figure 1.2). Regarding the depth estimation, we get a zero-slope for  $\tau_p$  when  $\dot{z}_0 = 10$  m, this value giving us our estimate for the depth to the source.

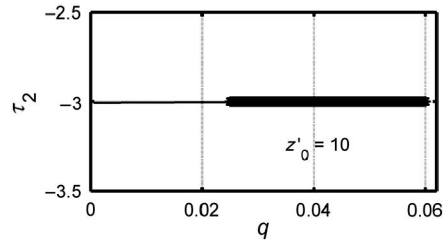


Figure 1.2: Scaling function for the second vertical derivative of the SP of a point pole source. The intercepts indicate  $N_2=3$ ; i.e.,  $N=1$  for the SP (Table 1). The depth to the source  $z_0$  is given by the value of  $\dot{z}_0$  yielding the zero-slope for  $\tau_2(q, \dot{z}_0)$ ; that is,  $\dot{z}_0=10$  m.

### 1.5 Synthetic Examples

The SP anomalies produced by some simple polarized geological structures may be conveniently expressed by the general equation (Yüngül, 1950; Bhattacharya and Roy, 1981; Abdelrahman and Sharafeldin, 1997)

$$S(x, z) = K \frac{(x-x_0) \cos \theta + (z-z_0) \sin \theta}{((x-x_0)^2 + (z-z_0)^2)^m} \quad (1-15)$$

where,  $z_o$  is the depth of the body,  $\theta$  is the polarization angle between the axis of polarization and the horizontal,  $K$  is the magnitude contrast of the polarization electric dipole moment,  $x$  is the horizontal position coordinate, and  $m$  is the shape factor, a quantity related to the shape of the buried structure which is similar but not equal to the structural index. The shape factors for a sphere (3D), a horizontal cylinder (2D), and a semi-infinite vertical cylinder (2D) are 1.5, 1.0, and 0.5, respectively. The shape factor approaches zero as the structure approaches a horizontal sheet and 1.5 when the structure becomes a sphere. The shape factor is related to the structural index by a known relationship:  $N=2m-1$  (Roy, 2001).

Let us first consider isolated sources. SP anomalies are computed from equation (1-15) with the following parameters: 1) Sphere model with  $K=-600$  mV,  $\theta=90^\circ$  and  $z_o=30$ m (Figure 1.3a), and 2) Horizontal cylinder model with  $K=-300$  mV,  $\theta=45^\circ$  and  $z_o=10$ m (Figure 1.4a). We used equation (1-9) to compute the DEXP transformed fields for the sphere model from the first vertical derivative of the self-potential (Figure 1.3). The geometrical method yields a good estimate of the depth to the source,  $z_o=30$  m, at the position where the ridges intersect each other. The scaling exponent was determined (Figure 1.3d) accurately by analysing the scaling function for a selected ridge, yielding  $N_l=3$ , i.e.  $N=2$ , corresponding to the right type of source (Table 1.1). Using this value and equation (1-13), we then formed the DEXP transformation of the field (Figure 1.3c) and estimated the depth to the causative source at its extreme, a low at 30 m depth (white marker). This result confirms the estimate obtained with the geometrical and scaling function methods. Let us now consider the horizontal cylinder model (Figure 1.4). First, we applied the geometrical method by computing the ridges (cyan lines) for the 1<sup>st</sup> order vertical derivative of the SP (Figure 1.4a). Once again the first-order vertical derivative was chosen in order to obtain a consistent number of ridges. Note that ridges are now not symmetrically disposed as in the sphere case. This is because we assumed a  $\theta=45^\circ$  dip for the polarization. Nevertheless, the ridges (Figure 1.4b) clearly indicate the

depth to the source intersecting each other at the right 10 m depth. Note that the symmetry of the ridge set may be used as diagnostic for determining the dip of the dipole moment.

The scaling function is computed for the ridge at  $x=106$  (Figure 1.4d) giving  $N_I=2$ , i.e., an  $N=1$  structural index estimate, so indicating rightly the nature of the source (horizontal cylinder, see Table 1.1). Using equation (1-13) again we formed the DEXP transformed field, shown in Figure 1.4c. We may immediately notice that in this case there are two extreme points: a low and a high, because the dipole polarization is not vertical. The depth estimate is nevertheless well deduced by both the extreme positions.

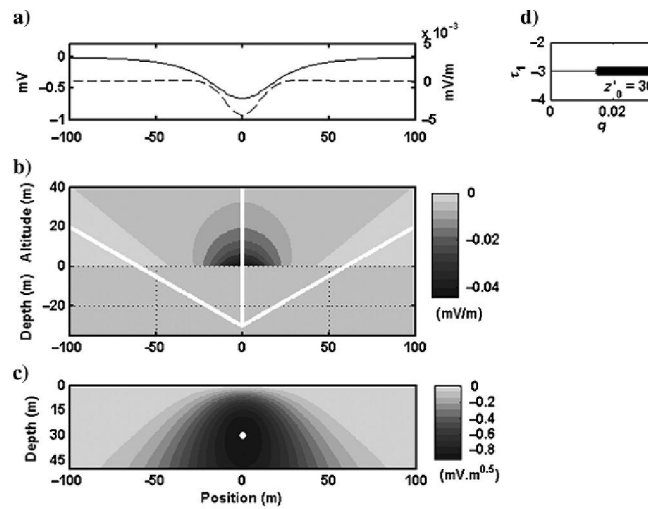


Figure 1.3: The DEXP of the first vertical derivative of the SP anomaly of a polarized sphere. (a) The SP anomaly (solid line) and its first-order vertical derivative (dashed line), (b) first vertical derivative up to  $z = 40$  m and ridges (white solid lines): they intersect at the source position (30 m depth), (c) first-order DEXP transformation, the minimum (white dot) is at the right depth to the source, (d) scaling function for the central ridge: the intercept indicates  $N_1 = 3$ , i.e.,  $N = 2$ , and the depth to the source  $z_0$  is given by the value of  $z'_0$  yielding the zero-slope for  $\tau_1(q, z'_0)$ , that is,  $z'_0 = 30$  m.

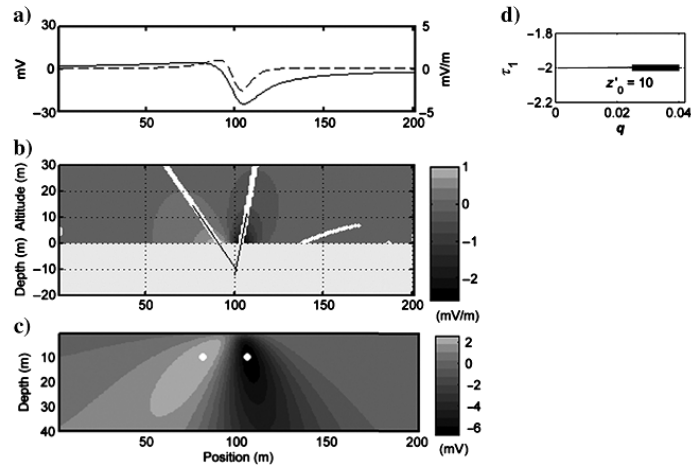


Figure 1.4: The DEXP of the first vertical derivative of the SP anomaly of a polarized horizontal cylinder. (a) SP anomaly (solid line) and its first-order vertical derivative (dashed line), (b) first vertical derivative at different altitudes and ridges (white solid lines), which intersect at the right source position, (c) first-order DEXP transformation: the extreme points (white dots) indicate the depth to the source, (d) scaling function for the central ridge: the intercept indicates  $N_1 = 2$ , i.e.,  $N = 1$ , and the depth to the source  $z_0$  is given by the value of  $z'_0$ , yielding the zero-slope for  $\tau_1(q, z_0)$ ; that is,  $z_0 = 10$  m.

In the next example we test the effect of the noise on the results of the DEXP method. We used the same horizontal cylinder as in the previous example, with addition of 5% white noise (Figure 1.5). Looking at the ridges (b) it is clear that they appear slightly perturbed only at very low scales, so not affecting the depth estimation with the geometric method. This behaviour is confirmed also in the case of the DEXP transformation (c) where the depth of the horizontal cylinder is again well estimated at the extreme points.

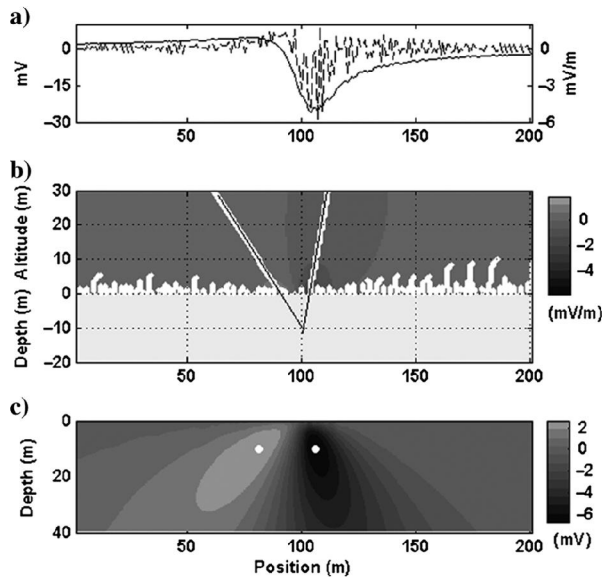


Figure 1.5: The DEXP of the first vertical derivative of the SP anomaly of a polarized horizontal cylinder contaminated with 5% Gaussian noise. (a) The SP anomaly (solid line) and its first-order vertical derivative (dashed line), (b) first vertical derivative at different altitudes and ridges (white solid lines), which intersect at the source position. We note that the added noise only affects ridges at the lowest scales, letting the ridges indicate safely the source position as well, (c) first-order DEXP transformation: the extreme points (white dots) indicate the depth to the source at 10 m.

Finally we test the efficiency of the method with a multi-source model (Figure 1.6). In order to do this, we used SP data of two sources; a vertically polarized sphere and a horizontal cylinder, with the following parameters: (1) Sphere model with  $K=-500$  mV,  $\theta=90^\circ$ ,  $x=120$ ,  $y=41$  and  $z_o=10$  m, and (2) horizontal cylinder model with  $K=-200$  mV,  $\theta=90^\circ$ ,  $x=80$  and  $z_o=20$  m.

The model is sized (201m x 201m x 40m) with 1 m horizontal step and 0.2 m altitude-step. With a PC with a 2.0 GHz processor, the DEXP transformation required only 97.79 seconds to be computed. Interference effects are dominant in the SP of this model (Figure 1.6a, left) but by increasing the order of differentiation this effect is substantially reduced

(Figure 1.6a, center and right). Regarding the geometrical method, Figure 1.6 clearly shows that we need to analyze at least the second-order derivative of the SP to warrant a sufficient number of well-resolved ridges for both sources. For the horizontal cylinder the ridges are already well developed at the first derivative, while the 2<sup>nd</sup> order derivative show better-resolved ridges for the sphere. We made similar considerations in order to estimate the structural index: for the horizontal cylinder, we selected the vertical ridge at  $x=81$ , and estimated  $N_1 = 2$ , i.e.,  $N=1$  (Figure 1.6c, left); for the sphere we selected the vertical ridge at  $x=121$ , estimating  $N_2 = 4$  (Figure 1.6c, right), i.e.,  $N=2$ . Both the estimated values agree with those for their own source-type (Table 1.1).

We note finally, also, that also the resolution of the DEXP images increases with the order of differentiation (Figures 1.6d; e). We must however take into account the DEXP theory in order to get correct depth estimations. In fact,  $N=1$  is the right value for estimating the depth of the horizontal cylinder (Figure 1.6d, left,  $p=0$ ; center,  $p=1$ ; right,  $p=2$ ) but is not appropriate for the sphere (Table 1.1), for which a shallower depth is estimated. Conversely, when we use  $N=2$ , the DEXP images show a correct depth for the sphere and too deep a depth for the horizontal cylinder (Figure 1.6e, left:  $p=0$ ; center:  $p=1$ ; right,  $p=2$ ). This indicates the importance of estimating the appropriate structural index for calculating the scaling-law for imaging methods such as DEXP. At the same time this gives the DEXP method a clear advantage over other methods, such as the cross-correlation or the migration, which behave as assuming a single and prefixed value for the structural index (Fedi and Pilkington, 2012), no matter different kinds of sources are present.

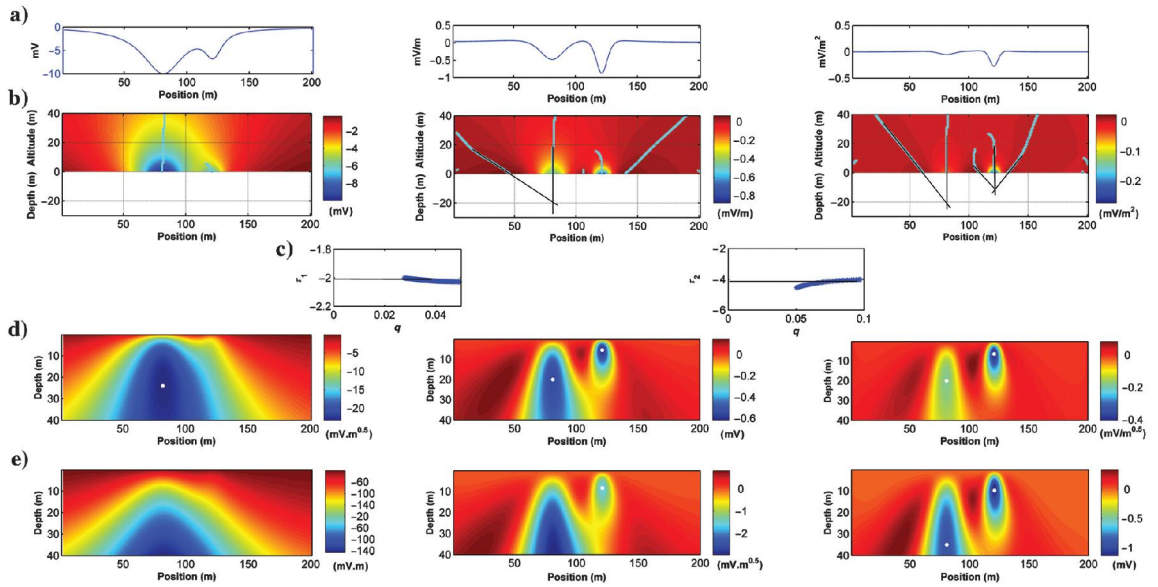


Figure 1.6: The DEXP method applied to a multisource model. (a) The SP anomaly (left), its first vertical derivative (center), and its second vertical derivative (right), (b) the continued sections of the different order of derivatives (left,  $p = 0$ ; center,  $p = 1$ ; right,  $p = 2$ ), (c) scaling functions for the horizontal cylinder (left) calculated along the vertical ridge at  $x = 81$  m of the first-order derivative,  $N_1 = 2$ , i.e.,  $N = 1$ , and for the sphere (right) calculated from the vertical ridge at  $x = 121$  m of the second-order derivative,  $N_2 = 4$ , i.e.,  $N = 2$ , (d) DEXP images calculated using  $N = 1$  for the SP anomaly (left), its first vertical derivative (center), and its second vertical derivative (right), (e) DEXP images calculated using  $N = 2$  for the SP anomaly (left), its first vertical derivative (center), and its second vertical derivative (right).

## 1.6 Field Examples

In this section we apply the DEXP method to the SP anomalies of some real cases.

### A) Malachite Mine, Colorado, (USA):

We analyzed the self-potential anomaly profile described in (Dobrin, 1960, Abdelrahman et al., 2004) over the Malachite Mine, Jefferson County, Colorado. The SP anomaly measurements were performed and described by Heiland et al. (1945). This anomaly profile is due to a nearly vertical cylindrical massive sulphide ore body, approximately 11 m

wide and buried at about 13.7 m depth, according to drilling information (Heiland et al., 1945).

The anomaly is digitized with a 1 m step, and continued with a 0.2 m step until 25 m altitude (Figure 1.7). We estimate the structural index by calculating the scaling function for the ridge at  $x=83$ . Looking at the intercept, the estimated structural index value  $N_3$  equals 3.5, i.e.,  $N$  equals 0.5, indicating a source model which may be explained as a polarized vertical cylinder quite extended along the horizontal direction, this being in agreement with the geometry of the source, as resulting from drillings. DEXP and geometrical methods (order 3) both yield about 13.6 m for the depth to the source (Figure 1.7b; c) and this is in agreement with the known drilling depth, as it was mentioned above.

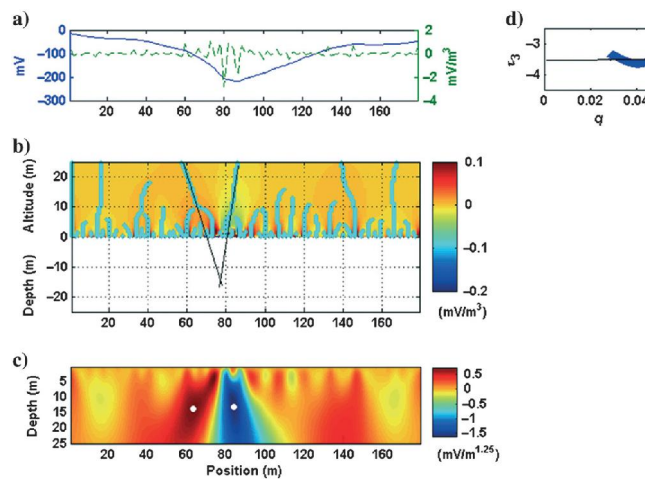


Figure 1.7: The DEXP method for the SP anomaly profile over the Malachite Mine, Jefferson County, Colorado, USA: (a) the SP profile (blue solid line) and its third-order vertical derivative (green dashed line); (b) third-order vertical derivative of the SP anomaly at different altitudes and ridges (cyan solid lines): the selected ridges intersect each other at about 13.6 m depth; (c) DEXP transformation of the third-order vertical derivative of SP: the extreme point (white dot) also indicates a 13.6 m source depth; (d) scaling function of the ridge on the right yielding  $N_3 = 3.5$ , i.e.,  $N = 0.5$ .

B) *The Sariyer anomaly (Turkey):*

Yüngül (1950) describes an SP survey in the Sariyer area (Turkey), which led to the discovery of a sulfide mass containing zones with copper concentration as high as 14%. The depth to the sulfide mass is about 25 m, as obtained from the data from boreholes, shafts, and tunnels. The anomaly is digitized with a 1 m step and continued with a 0.2 m step until 40 m altitude (Figure 1.8). The structural index is estimated by calculating the scaling function for the ridge at  $x=73$  (b). Looking at the intercept (d), the estimated structural index value  $N_2=3$ , i.e.,  $N=1$ , so indicating a source model which could be explained as a polarized cylinder. The DEXP method (order 2) and the geometric method yield 23.2 m for the depth to the source in good agreement with the known drilling depth (Figure 1.8b; 1.8c).

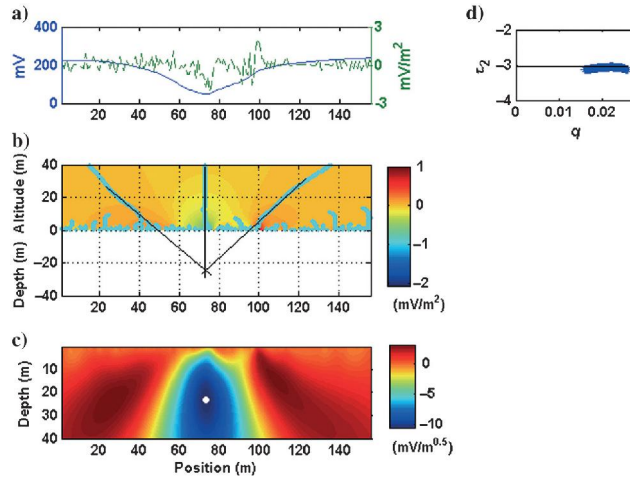


Figure 1.8: The DEXP method for the SP anomaly profile in the Sariyer area, Turkey. (a) SP profile (blue solid line) and its second-order vertical derivative (green dashed line), (b) second-order vertical derivative of the SP anomaly at different scales and ridges (cyan solid lines): the selected ridges intersect each other at 23.8 m depth, (c) DEXP transformation of the second-order vertical derivative SP: the extreme point (white dot) also indicates a 23.8 m source depth, and (d) scaling function of the central ridge, showing  $N_2 = 3$ ; i.e.,  $N = 1$ .

### C) Bender anomaly (India)

Here we interpret the Bender anomaly (Figure 1.9), Balangir, Orissa, India (Bhattacharya et al., 1984, 2007). The rock units in the area are mainly of the Archaean crystalline complex; garnetiferous illuminite schists, gneisses and garnetiferous quartzites traversed by quartzite and pegmatite veins. In most parts, the rocks are covered by laterite and alluvium. The most important occurrence of graphite is graphite veins associated with pegmatites. The deposits are shallow and the ore was extracted by open cast mining and the actual depth to the top was 5 m. The open cast mine stopped due to flooding by groundwater but the presence of the ore is still seen at the bottom of the abandoned mine (Bhattacharya et al., 1984). Bhattacharya et al. (2007) interpreted this anomaly and computed COP and DOP maps from SP cross-correlation. However, they obtain inconsistent results, yielding a much deeper result in the DOP case (their figure 3). A main problem is that the cross-correlation method does not allow us to judge which result is the best, since the scanning function (related to a pole source and a dipole source for COP and DOP, respectively) is not estimated, but a priori assumed.

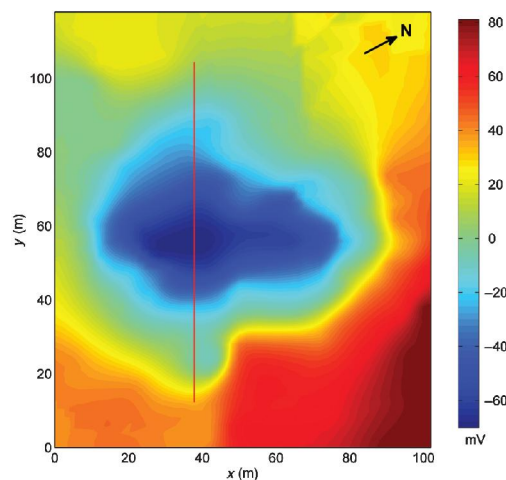


Figure 1.9: Self-potential Bender anomaly map, India. The red solid vertical line indicates the selected profile chosen to represent the DEXP transformed field.

According to what is shown in this work, the DEXP method instead allows the depth to be determined in a more objective way. The scaling law is in fact not assumed but computed on the basis of our estimation of the structural index, as far as the scaling function  $\tau$  is analysed before performing the DEXP transformation. The anomaly was digitized with 1 m interval (Figure 1.9). The structural index was then estimated by calculating the scaling function for the central ridge (Figure 1.10b) of the first-order vertical derivative of the SP (Figure 1.10a, green line). The number of ridges is in this case not sufficient to yield an estimate of the depth to the source with the geometrical method. Looking at the intercept (Figure 1.10d), the estimated structural index was estimated as  $N_I=2$  i.e.  $N=1$  (equation 1-12), so indicating a polarized horizontal cylinder source-model (Table 1.1). The DEXP method ( $p=1$ ) yields 16.8 m for the depth to the centre of the source (Figure 1.10c), in agreement with Agarwal and Srivastava (2009). Finally, we used the estimated structural index to scale the SP anomaly and produce a 3D representation of the DEXP transformed SP (Figure 1.11). The low area around 16.8 m yields a nice picture of the causative source at its correct depth.

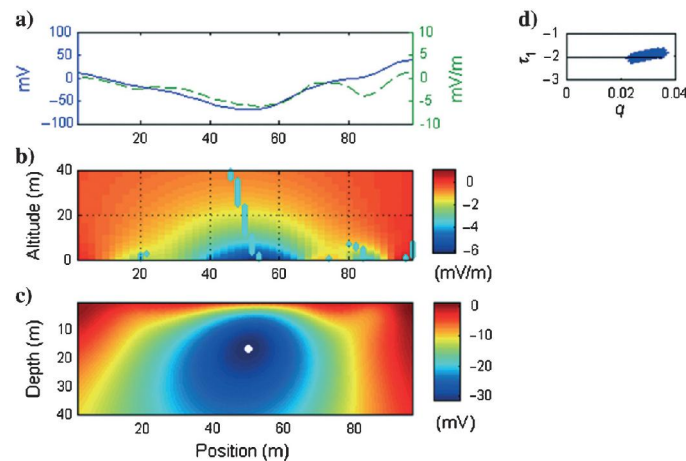


Figure 1.10: DEXP method for the SP profile of the Bender anomaly. (a) The SP profile (blue solid line) and its first vertical derivative (green dashed line), (b) first-order vertical derivative of the SP anomaly at different scales and ridges (cyan solid lines), (c) DEXP transformation of the first-order vertical derivative of SP: the extreme point (white dot) indicates 16.8 m

depth to the center of the source, and (d) scaling function of the first-order vertical derivative of the SP anomaly, from which we estimate  $N_1 = 2$ , i.e.,  $N = 1$ .

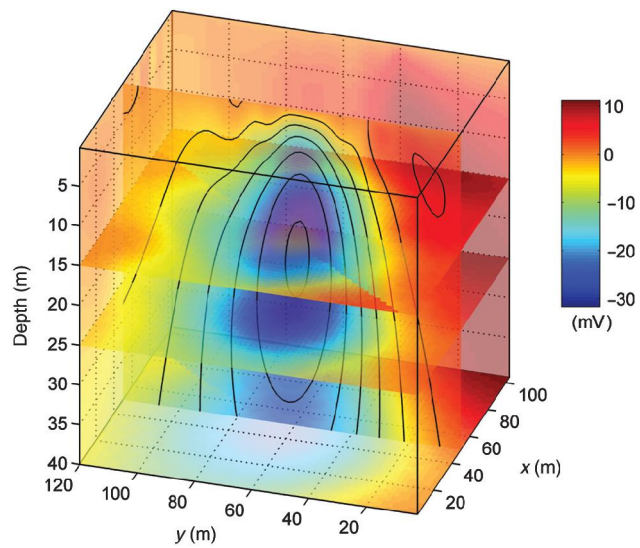


Figure 1.11: The 3D DEXP transformation of the SP Bender anomaly map. Contour lines along the central slice indicate the depth to the source at the local minimum.

## ***Chapter 2***

### ***Application of the DEXP method to the streaming potential data.***

#### **2.1 Introduction**

The self-potential anomalies have two main mechanisms; the oxidation-reduction associated with ore deposits and streaming potential (SP) associated with ground water flow through the electrokinetic coupling (Revil et al., 2004). There are two approaches for interpreting the origin of the SP anomalies related to ground water flow. The first approach supposes that SP signals could be mainly related to the thickness of the unsaturated (vadose) zone in which water penetrate vertically until the water table (Zablocki, 1978; Jackson & Kauahikaua, 1987; and Aubert et al., 1993). Another approach presumes that the main SP contribution is located along the water table and that the variations of the hydraulic head are directly responsible for the electrical potential anomalies measured at the ground surface (Fournier, 1989; Revil et al., 2004).

The SP anomalies have been interpreted by direct and inverse methods. The self-potential surface (SPS) method (Aubert and Atangana, 1996), wavelet transform (Sailhac and Marquis, 2001) and cross-correlation method (Patella, 1997a & 1997b, Revil et al., 2003) are examples of direct methods. On the other hand, several inversion techniques have been developed for the SP anomalies (e.g., Darnet et al., 2003; Fernández-Martínez et al., 2010, Jardani et al., 2006; Jardani et al., 2009).

In the cross-correlation method, the SP anomalies are interpreted through cross-correlation of the field with that by assumed elementary scanning-sources, e.g. a point-source by Patella (1997a, b) or a dipole-source by Revil et al. (2001) and Iuliano et al. (2002). The zero-lag cross-correlation may be mapped at different depths and horizontal positions of the scanning-source, so describing a possible distribution of source-density, this depending

however on the a priori type of scanning-source used, e.g. a single pole, a dipole or any other. The cross-correlation method was however shown to be equivalent to a multiscale approach (Gilbert and Sailhac, 2008; Fedi and Pilkington, 2012). Furthermore, an inherent lack of criteria was pointed out, to assess the best type of scanning-source (Gilbert and Sailhac, 2008).

In this chapter, we consider the application of a different multiscale method; the Depth from EXtreme Points (DEXP) method (Fedi, 2007; Fedi and Abbas, 2013), for the interpretation of the streaming potential data related to the flow of ground water.

## 2.2 Theory

Considering that the SP sources are along the water table (Figure 2.1), the electric potential  $U(r)$  (in mV) measured at the point  $P(\mathbf{r})$  located on the Earth's surface is related to the hydraulic head  $h$  at point  $M(\mathbf{r}_q)$  at the water table (in m) by a Fredholm equation of the first kind (Fournier, 1989; Revil et al., 2004),

$$U(r) = \frac{c'}{2\pi} \int_{\partial\Omega} h(\mathbf{r}_q) \frac{(\mathbf{r}-\mathbf{r}_q) \cdot \mathbf{n}(\mathbf{r}_q)}{|\mathbf{r}-\mathbf{r}_q|^3} dS \quad (2-1)$$

where  $\mathbf{n}$  is the unit normal vector over the water table  $\partial\Omega$ ,  $dS$  is a surface element of the water table,  $c'$  is an apparent streaming potential coupling coefficient (in mV m<sup>-1</sup>) given by  $c' = \theta C - C_s$ , where  $C$  and  $C_s$  are the electric potential coupling coefficients of the vadose and saturated zone respectively.  $\theta$  is the ratio between the electrical conductivity of the saturated and unsaturated zones (Revil et al., 2004).

For a 2D profile, assuming that the variation in  $y$  direction can be neglected, the electric potential is obtained by (Revil et al., 2004):

$$U(r) = \frac{c'}{2\pi} \int_0^L h(\mathbf{r}_q) \frac{(\mathbf{r}-\mathbf{r}_q) \cdot \mathbf{n}(\mathbf{r}_q)}{|\mathbf{r}-\mathbf{r}_q|^2} d\xi \quad (2-2)$$

where  $\xi$  represents the curvilinear coordinate along the water table line.

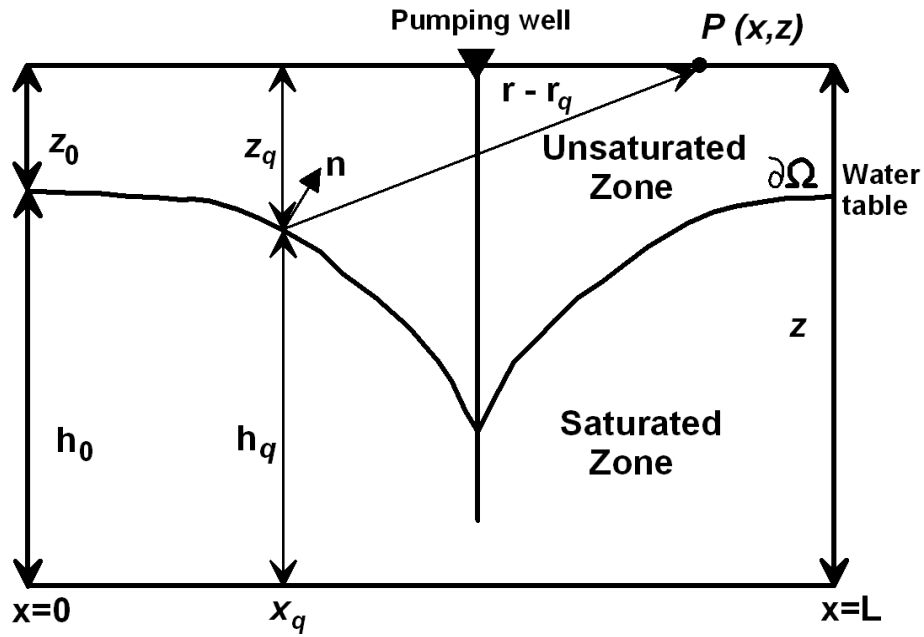


Figure 2.1: Sketch of the geometry of the water table for a pumping well (modified after Rizzo et al., 2004)

If we assume a flat measurement surface, so that  $\mathbf{n}$  is constant, equation (2-1) will be equivalent to the potential field due to a sheet or a simple layer (Baranov, 1975). Hence, as we mentioned in the previous chapter, the streaming potential has the same mathematical form as the magnetic potential. In fact, any deviation from the horizontal level of the water table can be interpreted as a one-point source (point-dipole, line of dipoles, or others). Consequently, we can apply the DEXP method to the streaming potential anomaly. The DEXP method is a multiscale method in which the potential or its derivative is continued and scaled with a scaling-law dependent on the geometry of the source. The scaling exponent is not fixed but can be determined directly from the data (Fedi, 2007; Fedi and Abbas, 2013). An important issue is that we do not need any a priori estimate of the hydraulic coupling coefficient; one more reason to use the DEXP method is that it is fast and stable.

Let us assume Cartesian coordinates where  $x$  and  $z$  are the horizontal and vertical directions, respectively, and the depth is positive downward. We can discretize equation (2-2)

in terms of the depths of the dipoles along the water table  $z_q$  assuming a vertical electric polarization as:

$$U(r) \approx -\frac{c'd}{2\pi} \sum_{q=1}^Q (z_q - z_0) \cdot \frac{z_q}{(x-x_q)^2 + z_q^2} \quad (2-3)$$

where  $d$  is the horizontal step. We can note from equation (2-3) that the two above-mentioned approaches for the origin of SP anomalies are in fact equivalent.

We have already said that any deviation from the horizontal level of the water table can be interpreted as a point source (point-dipole, line of dipoles, or others) so that the DEXP transformation (Fedi, 2007 and Fedi and Abbas, 2013) can be applied. The DEXP transformation  $\Omega_p$  is given by Fedi (2007) as:

$$\Omega_p(z) = z^{N_p/2} U_p(z) \quad (2-4)$$

where  $U_p$  is the  $p$ -th order derivative of  $U$  and  $z$  is the scale or altitude. The depth to the water table can be estimated from the extreme points of the DEXP image  $\Omega_p$ . In case of non-vertical polarization, the DEXP transformation can be applied to the analytic signal modulus of the SP anomaly. This is equivalent to the dipole occurrence probability (DOP) of Revil et al. (2001) but, once more, in an easier way: we do not need normalization. We also do not use a fixed scaling exponent (Fedi and Pilkington, 2012), which makes the DEXP method more suitable to be used in different situations.

The application of the DEXP transformation method requires upward continuation and vertical differentiation of order  $p$  for the computation of  $U_p$  and  $\Omega_p$ . As already said in the previous chapter, the upward continuation is not allowed for SP anomalies, being the air infinitely resistive. However, the upward continuation of SP data, from a measurement level  $z_m$  to the level  $z_m+a$ , is equivalent to the SP data at  $z_m$  of the same source located not at the

depth  $z_0$  but at the deeper depth  $z_0+a$ . In this way, the concept of vertical derivative of SP data may be introduced for SP anomalies as well (Fedi and Abbas, 2013).

### **2.3 Synthetic Example**

The SP anomaly of the water table model shown in Figure 2.2b is calculated using equation (2-3) . The SP anomaly (Figure 2.2a) was upward continued from 0 to 60 m and its 2<sup>nd</sup> order vertical derivative is calculated. Figure 2.3a shows the continued derivative with the ridges. The scaling function was calculated along two ridges at horizontal distances 500 m and 100 m (Figure 2.3b, c). Both scaling functions yield a scaling exponent equal 0.6. The scaling functions calculated along the two other ridges in the central part of Figure 2.3a did not give reasonable values of homogeneity degree due to the interference effects connected to the complexity of the source in this part.

I used the estimated scaling exponent to calculate the DEXP image shown in Figure 3.4a. The extreme points of the DEXP image give a good estimate of the depth of the water table. Also, I used the geometrical method to estimate the depth to the water table at the intersection of the ridges of the 4<sup>th</sup> order derivative of the SP anomaly (Figure 3.4b), this order warranting a nice degree of resolution to the problem. The results agree well with the true model of the water table.

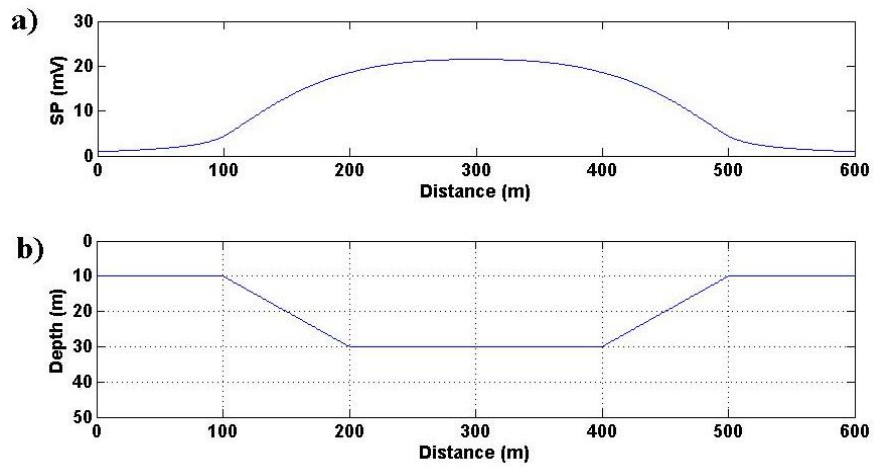


Figure 2.2: The SP anomaly of a water table model. (a) The SP anomaly, and (b) the depth to the water table.

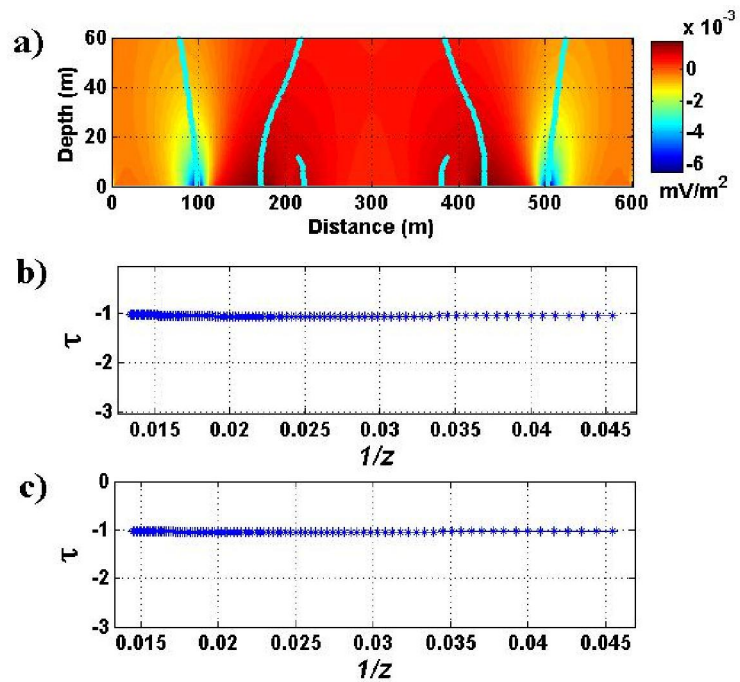


Figure 2.3: Scaling function analysis. (a) The upward-continued 2<sup>nd</sup> order derivative of the SP anomaly and its ridges, (b) the scaling function along the ridge at distance 500 m and (c) the scaling function along the ridge at distance 100 m.

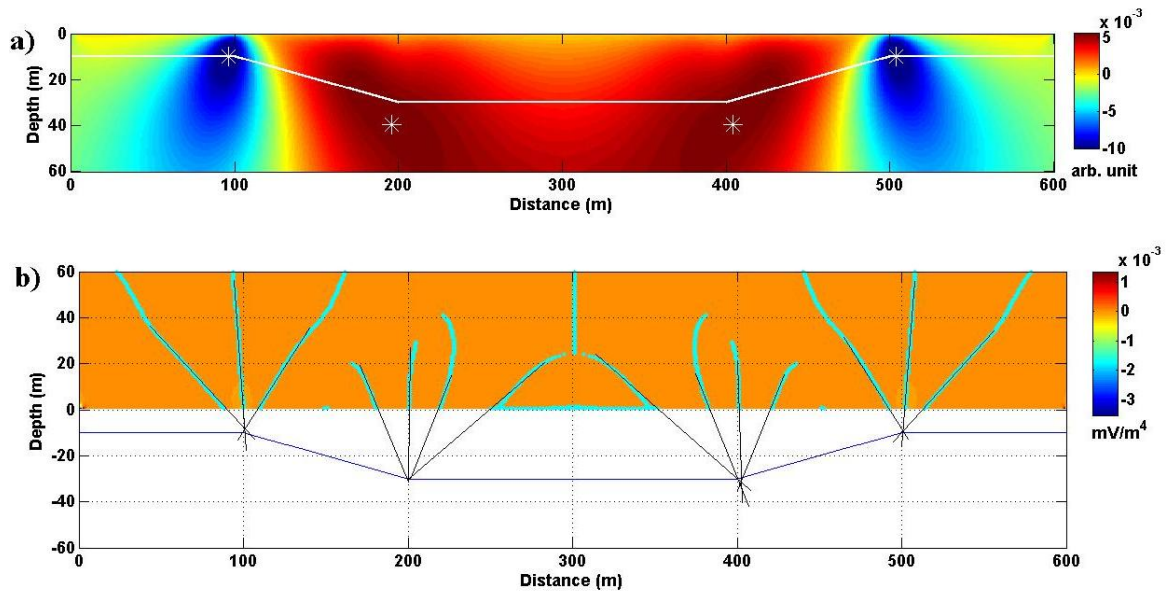


Figure 2.4: Application of the DEXP method and geometrical method for the estimation of the depth to the water table. (a) DEXP image calculated with the scaling exponent equal to 0.6; white stars indicate the estimated depths (b) the depth to the water table estimated by the geometrical method.

## 2.4 Real Examples

### 2.4.1 Well pumping test:

The DEXP imaging is applied to the streaming potential data collected near a pumping well from Bogoslovsky and Oglivy (1973). Figure 2.5 shows the SP anomaly over the pumping well (K-1) and also the piezometric depths. We note a positive anomaly with a symmetric form over the well location and other two small negative anomalies related to the infiltration from the surface drainage ditches.

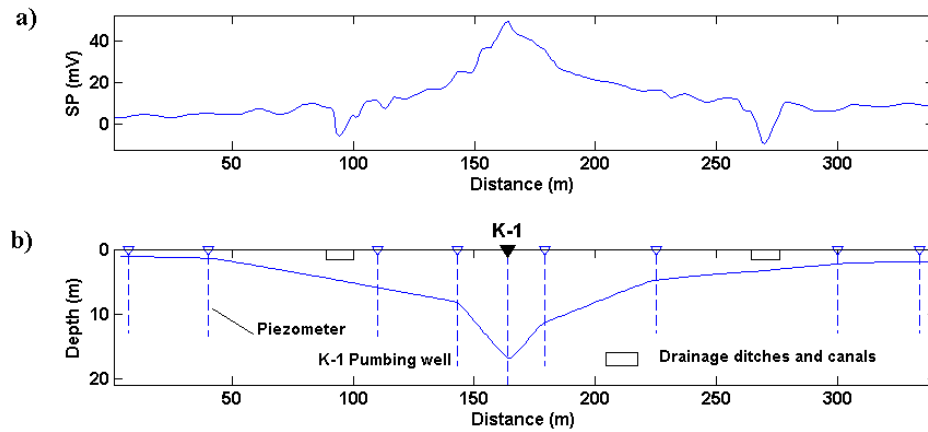


Figure 2.5: The streaming potential data profile near a pumping well (a) and the piezometric depths (b) after Bogoslovsky & Oglivy, 1973.

First, the 1<sup>st</sup> derivative of the SP anomaly is continued from 0 to 30 m with a 0.2 m vertical step (Figure 2.6a). Then the values of scaling exponent is estimated by analyzing the scaling function along a vertical ridges at  $x=\{95, 163, 270\}$  m (Figure 2.6d,e,and f). We found that the central positive anomaly over the pumping well and the negative anomaly related to the infiltration of the water in the subsurface at  $x= 270$  m need both a 0.9 scaling exponent, whereas the negative anomaly related to the infiltration of water in the subsurface at  $x= 95$  m needs a 1.15 scaling exponent. Finally, we obtained two DEXP images with the two estimated values of scaling exponents (Figure 2.6b and c). The estimated depths to the water table, indicated by the white stars, agree well with the measured piezometric depths.

The geometrical method was also applied to the SP anomaly by converging the ridges of the 3<sup>rd</sup> order derivative of the SP anomaly to the source area. The results shown in Figure 2.7 agree well with the piezometric depth information. I deleted the ridges near the border and under the noise level to better rendering the results.

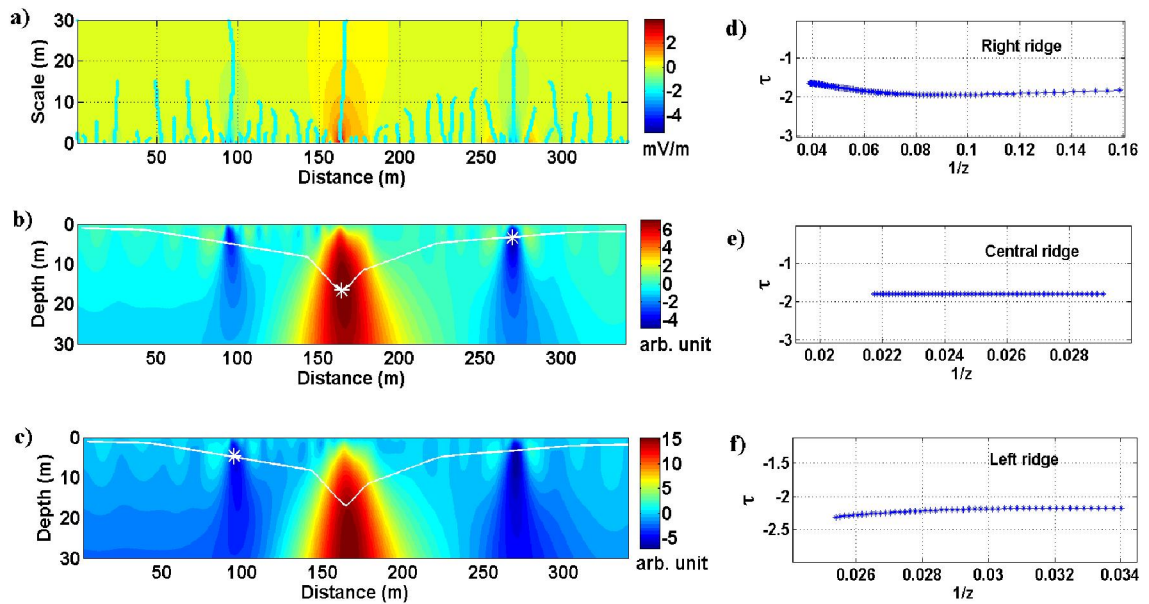


Figure 2.6: Application of the DEXP method to the SP data near a pumping well. a) The first-order derivative of the SP at different scales and ridges (cyan solid lines); b) DEXP image with 0.9 scaling exponent overlaid by the piezometric depths (white solid line); c) DEXP image with a 1.15 scaling exponent overlaid by the piezometric depths (white solid line); d) scaling function along the rightmost; e) scaling function along the central ridge; and f) scaling function along the leftmost ridge. White stars in b) and c) indicate the estimated depth to the water table.

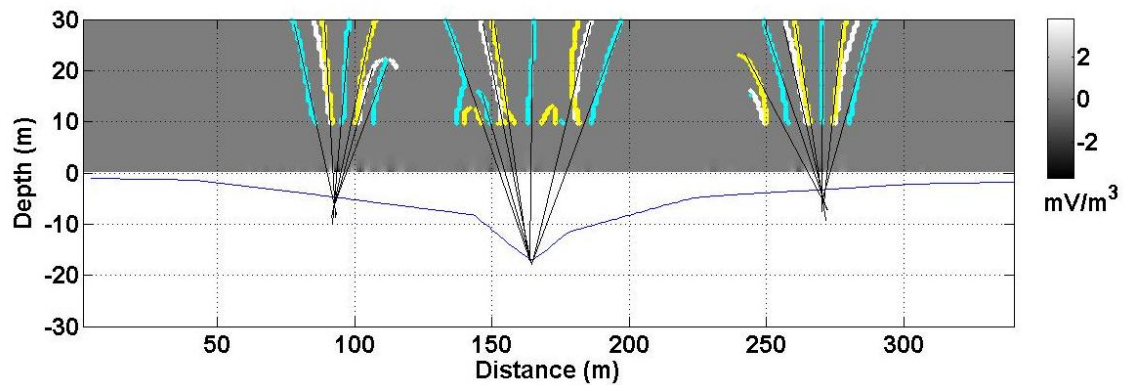


Figure 2.7: Application of the geometrical method to the SP anomaly in a pumping test. The solid blue line shows the piezometric depths.

### 2.4.2 Sinkhole detection:

Finally, we applied the multiscale approach for the detection and imaging of sinkholes. The DEXP transformation is applied to the SP data measured at San Vittorino Plain (Rieti), Central Italy (Cardarelli, et al., 2014). The study area is the San Vittorino Plain, located in Central Italy near the town of Rieti (around 80 km northern of Rome), along the Velino River Valley (Figure 2.8). Significant springs occur along the valley and along its right margin; the main springs (on the southern slope and at the northern boundary of the San Vittorino Plain) are the Peschiera springs exploited to supply drinking water to the city of Rome (Cardarelli, et al., 2014).

The San Vittorino Plain is an area of discharge of important fractured carbonate aquifers belonging to the meso-cenozoic carbonate platform domain. The carbonate bedrock is highly tectonized and overlaid by the heterogeneous alluvial deposits of the Velino River (Centamore et al. 2009). All the area is prone to piping sinkholes. The most important origin of this kind of sinkhole is the upwelling of water and gases from a karst bedrock within the alluvial overburden (Cardarelli et al., 2014).

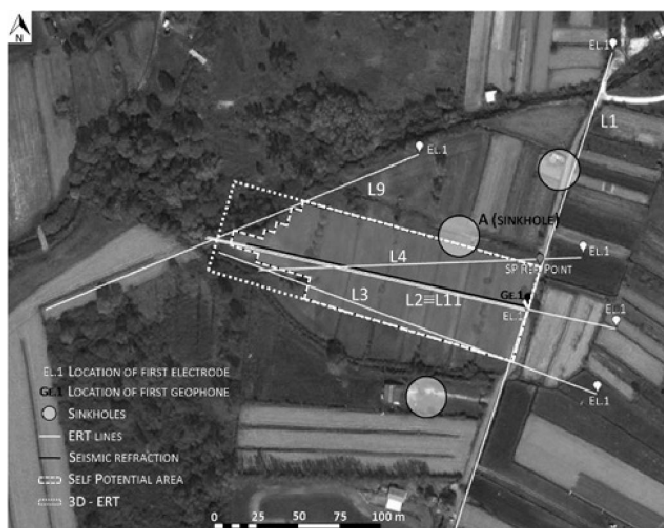


Figure 2.8: Aerial plan of the surveyed areas and map of the field investigations (After Cardarelli et al., 2014).

Figure 2.9 shows the residual SP map of the area and we can identify two strong negative anomalies, possibly related to sinkholes; the first along the profile AB and the second along the profile CD. Analyzing the scaling function for the analytic signal magnitude of SP data, we see values of the scaling exponent equal to 1.35 and 1.15 for profiles AB and CD, respectively (Figure 2.10a and c).

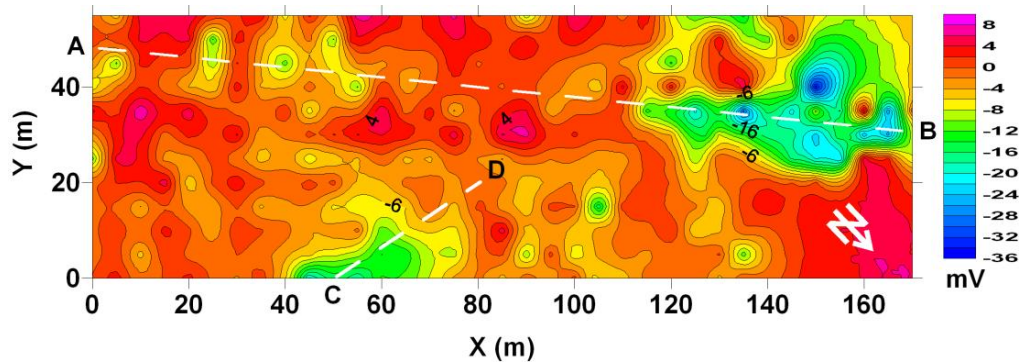


Figure 2.9: Residual SP map at San Vittorino Plain (Rieti), Central Italy. The dashed lines indicate the profiles used in the analysis.

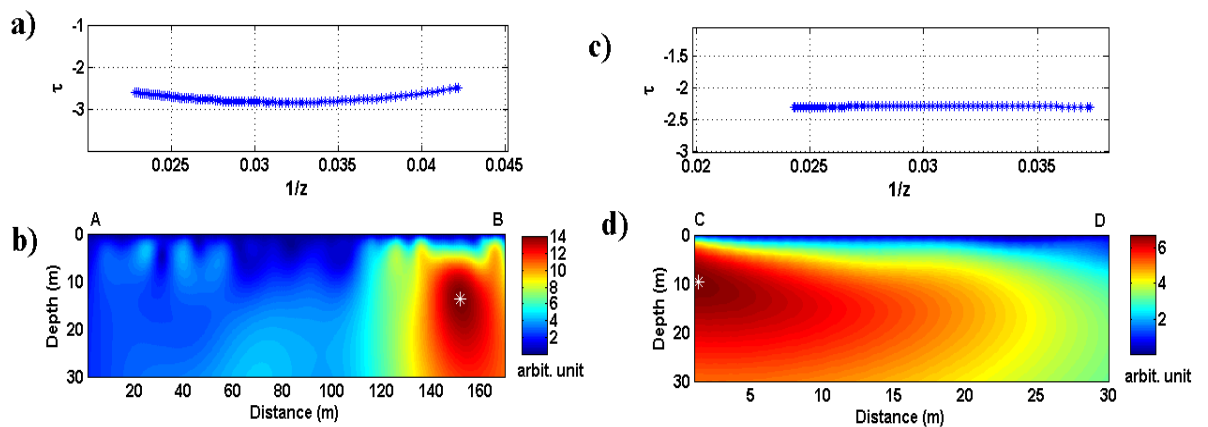


Figure 2.10: The DEXP imaging applied to the SP profiles at San Vittorino Plain (Rieti), Central Italy. a) The scaling function of a selected ridge along the AB profile; b) the DEXP image of the AB profile; c) the scaling function of a selected ridge along the CD profile; and d) the DEXP image of the CD profile. White stars in (b) and (d) indicate the estimated depth.

The DEXP images show depths to the sources equal to 13.8 and 9.6 m for profiles AB and CD, respectively (Figure 2.10b and d). Finally, the average of the estimated scaling exponent is used to make a 3D DEXP transformed volume of SP data (Figure 2.11). It shows clearly the position of two sinkholes. These results agree well with that obtained by Cardarelli et al. (2014) using the SPS method for the interpretation of SP data, and confirmed by the resistivity and seismic methods.

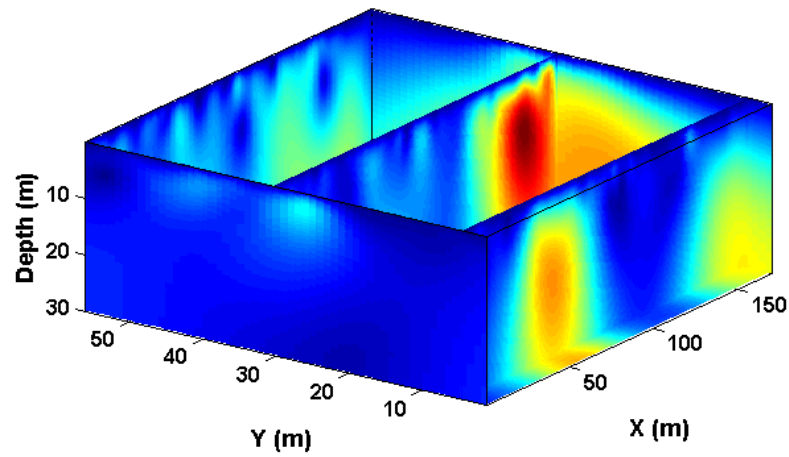


Figure 2.11: 3D DEXP volume of the analytic signal magnitude of the SP map at San Vittorino Plain (Rieti), Central Italy.

## ***Chapter 3***

### ***Automatic DEXP Imaging of Potential Fields Independent of the Structural Index.***

*This chapter is published as: Abbas, M. A., and Fedi, M. (2014). Automatic DEXP imaging of potential fields independent of the structural index. *Geophysical Journal International*, 199 (3), 1625-1632.*

#### **3.1 Introduction:**

Automatic or semi-automatic interpretation of potential field data is supported by many methods, such as Euler deconvolution (Thompson, 1982; Reid et al., 1990), or others based on the horizontal gradient function applied to gravity and pseudo-gravity and reduced to pole magnetic data (Cordell and Grauch, 1985; Roest et al., 1992), analytic signal magnitude (Nabighian, 1972) (or total gradient) applied to magnetic data, and the local wavenumber method applied to magnetic data (Thurston and Smith, 1997; Smith et al., 1998). Hsu et al. (1998) used the ratio between the moduli of the second and first-order analytic signals at two different altitudes to estimate depth to the source and structural index. Vallée et al., (2004), used the ratio of Poisson wavelet coefficients of the first and second orders, equivalent to the upward continuation of the analytical signal. Salem et al. (2002) estimated the depths to compact magnetic objects from the ratio of the analytic signal magnitudes of the magnetic anomaly and of the vertical gradient of the magnetic anomaly. These methods have a simple mathematical form for isolated sources; however, for non-isolated sources, the above-mentioned methods are no longer linear and suffer from the interference effects of the nearby sources.

Fedi (2007) introduced the Depth from EXtreme Points (DEXP) method in order to get depth and structural index estimates of the sources of potential fields and also provide images

of the source distribution (Fedi and Pilkington, 2012). The DEXP method consists of scaling the potential field, or its partial derivatives, with a specific power-law whose exponent is related to the structural index,  $N$ , a quantity related to the source geometry. The method has been applied to gravity, magnetic and self-potential data, to provide a fast image of the respective source distributions (see: Fedi, 2007; Fedi and Pilkington, 2012; Fedi and Abbas, 2013). Note that the structural index can be estimated in advance by several methods, based on the scaling function (Cella et al., 2009; Florio et al., 2009) or, alternatively, it may be assumed as equal to a value depending on the expected source.

We here propose a new version of the DEXP method, which has the notable improvement of using a power-law that does not depend anymore on the structural index of the sources. We will show that this feature makes it fully automatic, so that it may be implemented as a fast imaging method.

### 3.2 Theory

We use a Cartesian reference system, where  $x$ ,  $y$  and  $z$  follow the horizontal and vertical directions and the depth is positive downward. The key concept of the DEXP theory is the scaling function  $\tau$ , defined as the derivative of the logarithm of the potential field,  $f$ , or any of its  $p$ th-order vertical derivative  $f_p$ , with respect to the logarithm of  $z$  (Fedi, 2007):

$$\tau_p = \frac{\partial \log(f_p)}{\partial \log(z)}. \quad (3-1)$$

The scaling function assumes a simple form for homogenous fields. For instance, along the lines defined by the zeros of the field horizontal derivative, here called ridges (Fedi et al., 2009), it is simply expressed as:

$$\tau_p = -\frac{N_p z}{z - z_0} \quad (3-2)$$

In equation (3-2),  $z_0$  is the depth to the source and  $N_p$  is the opposite of the homogeneity degree of  $f_p$ , defined as:

$$N_p = N + p, \quad (3-3)$$

where  $N$  is the structural index, a quantity related to the geometry of the source (Thompson, 1982). We here adopt the convention to refer  $N$  to the opposite of the homogeneity degree of the magnetic field and, in the gravity case, to that of the gravity field. Note that the depth  $z_0$  may refer to the top of the source or to its centroid. For instance, in the magnetic case, for  $N=3$ ,  $z_0$  will refer to the center of the sphere, while for  $N=2$   $z_0$  will refer to the center in the case of an infinitely extended horizontal cylinder, and to the top in the case of a bottomless vertical cylinder. This is well known to Euler deconvolution practitioners (e.g. Hsu, 2002). Fedi (2007) defined the DEXP transformation  $\Omega_p$  as:

$$\Omega_p = z^{N_p/2} f_p \quad (3-4)$$

and showed that the DEXP transformation can be used to evaluate at its extreme points the depth to the source.

From equation (3-4), we note that the scaling law depends on the value of the structural index  $N$ . As shown by Fedi and Pilkington (2012), this feature makes this method more accurate than other imaging methods such as migration (Zhdanov, 2002), correlation (Patella, 1997) and others, which use a fixed weighting in their inherent scaling laws. The quality of the result depends on the selection of the appropriate  $N$ , which may either assumed or estimated before performing the transformation.

The method proposed in this paper is a modification of the DEXP method, based on applying the DEXP transformation (equation 3-4) to the ratio of two different-order vertical derivatives of  $f$ .

To show this, let us consider the ratio,  $\mathcal{R}_{mn} = f_m / f_n$ , between two different-order vertical derivatives of a homogenous field  $f, f_m$  and  $f_n$ , where  $m$  and  $n$  are the respective orders of differentiation. A little algebra shows that the scaling function of  $\mathcal{R}_{mn}$  may be simply obtained using equation (3-1):

$$\tau(\mathcal{R}_{mn}) = \tau\left(\frac{f_m}{f_n}\right) = \frac{\partial \log\left(\frac{f_m}{f_n}\right)}{\partial \log(z)} = \frac{\partial \log(f_m)}{\partial \log(z)} - \frac{\partial \log(f_n)}{\partial \log(z)} = \tau(f_m) - \tau(f_n) \quad (3-5)$$

Using now equations (3-2) and (3-3), we find that  $\tau(\mathcal{R}_{mn})$  takes the simple form:

$$\tau(\mathcal{R}_{mn}) = -\frac{(m-n)z}{z-z_0}. \quad (3-6)$$

So, equation (3-6) has the form occurring for homogeneous functions (Fedi, 2007), since  $\mathcal{R}_{mn}$  is a homogeneous function of degree  $-(m-n)$  away from the zeros of  $f_n$ . The key point in equation (3-6) is that the scaling function is independent from the structural index and depends only on a known quantity, that is the difference between the orders of the field derivatives  $f_m$  and  $f_n$ .

In particular, at  $z=-z_0$ , it is:

$$\tau(\mathcal{R}_{mn})\big|_{z=-z_0} = -\frac{(m-n)}{2}. \quad (3-7)$$

Fedi (2007) has shown that for homogeneous functions the value  $\tau(f)\big|_{z=-z_0}$  is the exponent of the power law used to build the DEXP transformation. So, using equation (3-7) we may easily form the DEXP-transformed field  $\Omega$  of the ratio  $\mathcal{R}_{mn}$  as:

$$\Omega(\mathcal{R}_{mn}) = z^{(m-n)/2} \mathcal{R}_{mn} \quad (3-8)$$

Since the exponent  $(m-n)/2$  is known, the estimation of the depth to the sources by the DEXP image of  $\mathcal{R}_{mn}$  is completely automatic. In fact, all the properties of the DEXP transformation hold and, as shown in Fedi (2007), the depth to the sources can be simply obtained by estimating the positions of the extreme points of  $\Omega$ , i.e. those of the DEXP image. This kind of automatic DEXP transformation can be obviously applied to the ratio between two different-order vertical derivatives of gravity field.

We may also build one more type of DEXP transformation, based on the  $l$ th-order vertical derivative of  $\mathcal{R}_{mn}$ . In fact, since the ratio  $\mathcal{R}_{mn}$  is homogeneous of order  $m-n$ , its  $l$ th-order vertical derivative will be homogeneous of order  $m-n+l$ . In this case, the scaling function and the corresponding DEXP transformation will be, respectively, given by:

$$\tau\left(\frac{\partial^l}{\partial z^l}(\mathcal{R}_{mn})\right) = \tau(\mathcal{R}_{mnl}) = -\frac{(m-n+l)z}{(z-z_0)} \quad (3-9)$$

and

$$\Omega(\mathcal{R}_{mnl}) = z^{(m-n+l)/2} \mathcal{R}_{mnl} . \quad (3-10)$$

To show how equations (3-8) and (3-10) could be used in order to make automatic DEXP transformations of potential fields, let us first consider the gravity field of a simple homogeneous source, an infinitely extended horizontal line source, with a 10 km depth, horizontal location  $x_0=100$  km, radius 1 km and density contrast 1 g/cm<sup>3</sup> (Figure 3.1a). The step is 1 km. The ratio,  $\mathcal{R}_{10}$ , between the first vertical derivative of the field and the field, and its first vertical derivative,  $\mathcal{R}_{101}$ , were computed up to 30 km, with a 0.2 km vertical step. Both the DEXP images of  $\mathcal{R}_{10}$  and  $\mathcal{R}_{101}$  (Figure 3.1b and 3.1c, respectively) show extreme points at a 10 km depth giving an accurate estimate of the true depth to the source.

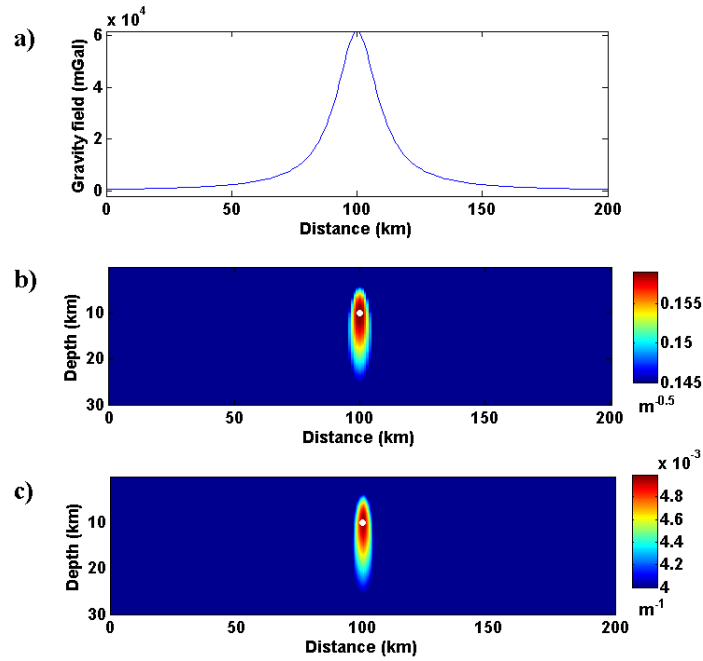


Figure 3.1: The automatic DEXP transformation applied to a gravity field of an infinite horizontal line source. a) The gravity anomaly field, b) the DEXP image of the ratio  $\mathcal{R}_{10}$  and c) the DEXP image of the vertical derivative of the ratio  $\mathcal{R}_{101}$ . White points indicate the estimated depth to the source.

The measured magnetic and self-potential fields' anomalies usually have a bipolar shape due to the inclination of polarization. Fedi (2007) showed that the DEXP transformation yields in this case a correct depth estimate looking at the extrema corresponding to both the low and high of the field (Fedi, 2007: fig. 5a-b). However, since in this case the horizontal source position is not well estimated, it could be convenient to perform the DEXP transformation of the analytical signal modulus instead, as shown in Fedi (2007, fig. 5c). In fact, in the 2D case, the analytical signal modulus is characterized by a bell-shape independent on the polarization and inducing field directions (Nabighian, 1972, Roest et al., 1992). Li (2006) shows that the 3D analytic signal amplitude slightly depends upon magnetization direction. Salem et al. (2002) showed that the ratio between the analytic signal moduli of the field and of the vertical derivative of the field is independent on the

magnetization direction. For these reasons we may take here into consideration the ratio between the analytic signal moduli of orders  $m$  and  $n$ . The analytical signal modulus  $|A|_p$  of  $f_p$ , assumes a simple form along ridges of type I (e.g. the lines formed by the zeros of the horizontal derivative of the field, Florio et al., 2009):

$$|A|_p = \left( \left( \frac{\partial f_p}{\partial x} \right)^2 + \left( \frac{\partial f_p}{\partial y} \right)^2 + \left( \frac{\partial f_p}{\partial z} \right)^2 \right)^{1/2} = \left| \frac{\partial f_p}{\partial z} \right| \quad (3-11)$$

So, for a isolated source, we have along ridges of type I:

$$\tau_p(|A|_p) = \frac{\partial \log(|A|_p)}{\partial \log(z)} = -(N_p + 1) \frac{z}{|z - z_0|} \operatorname{sgn}(z - z_0) \quad (3-12),$$

$$\text{where } \operatorname{sgn}(z - z_0) = \begin{cases} -1 & \text{if } z - z_0 < 0, \\ 0 & \text{if } z - z_0 = 0, \\ +1 & \text{if } z - z_0 > 0. \end{cases}$$

Since  $z - z_0$  is positive, we have that  $|A|_p$  is a homogenous function of degree  $-(N_p + 1)$ . We may so deduce that the scaling function of the ratio  $\mathcal{R}_{mn} = |A|_m / |A|_n$  is the same as that for the ratio  $f_m/f_n$  (equation 3-7). Consequently, we have that also equations (3-8) and (3-10) will hold. Here we have derived several new versions of the DEXP method; while in the gravity case we may just consider the ratio between two derivatives of the field, the ratio between two analytic signal magnitudes is recommended for magnetic field, in order to reduce the effects of the inclination of the field. The last version, based on scaling the derivative of the ratio, can be used in both cases, to further reduce interference effects.

Here, we considered the magnetic field of an infinite horizontal line of dipoles, with a 10 m depth, horizontal location  $x_0=100$  m and dipole moment  $1000 \text{ Am}^2$  (Figure 3.2a). Inclination and declination of both the inducing field and the magnetization vector are  $60^\circ$  and  $0^\circ$ , respectively. We computed the ratio  $\mathcal{R}_{21}$  between the second-order and first-order analytic

signal moduli of the field, and the ratio  $\mathcal{R}_{41}$  between the fourth-order and first-order analytic signal moduli of the field, with a 1 m horizontal step and a 0.2 m vertical step. Both the two DEXP images (Figures 3.2b and 3.2c) give a good estimate of the depth at 10 m.

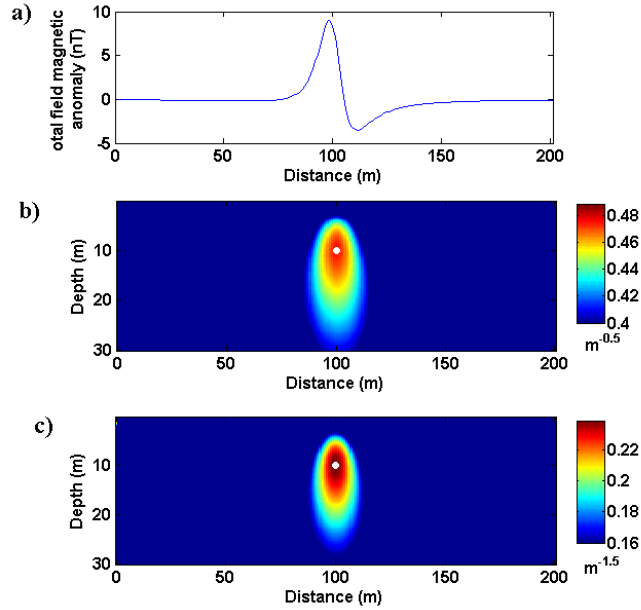


Figure 3.2: The automatic DEXP transformation applied to the magnetic field of an infinite horizontal line of dipoles. a) The magnetic anomaly field; b) the DEXP image of the ratio  $\mathcal{R}_{21}$  between the second-order and first-order analytic signal moduli of the field; c) the DEXP image of the ratio  $\mathcal{R}_{41}$  between the fourth-order and first-order analytic signal moduli of the field. White dots indicate the estimated depth to the source.

### 3.3 Estimation of the Structural Index

Once the depth is estimated automatically, the structural index may be easily determined by the scaling function (equation 3-2) at  $z=-z_0$ . We find in fact that:

$$\tau_p(f_p)\Big|_{z=-z_0} = -\frac{N_p z}{z-z_0}\Big|_{z=-z_0} = -\frac{N_p}{2} \quad (3-13)$$

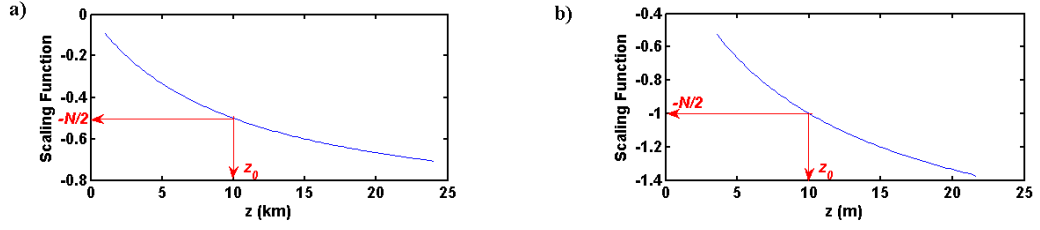


Figure 3.3: Estimation of the structural index using equation (3-13). (a) The scaling function of the gravity field of an infinite horizontal line source; (b) the scaling function of the magnetic field of an infinite horizontal line of dipoles. In both the figures we see that the values of the scaling function at  $z=-z_0$  yield the half of  $N_p$ , according to equation (3-13).

Our first example is the gravity field of an infinite horizontal line source. By analyzing the scaling function with respect to the altitudes, we may use equation (3-13) and find that, at  $z=-z_0=10$  km, the scaling function is  $-0.5$ , i.e. the structural index  $N$  equals 1 (Figure 3.3a), which is in agreement with the theoretical value. In the case of the magnetic field of infinite horizontal line of dipoles, using again equation (3-13), we found that, at  $z=-z_0=10$  m, the scaling function is  $-1$ , that is yielding  $N=2$  which is the correct theoretical value for the structural index of this source (Figure 3.3b).

Another method to estimate the structural index consists in using both the estimated depth and the value of the DEXP extreme points. We will find at  $z=-z_0$ :

$$\Omega_{\max} = \Omega|_{z=-z_0} = \frac{\prod_{p=n}^{m-1} N_p}{2^{m-n} (z_0)^{(m-n)/2}} \quad (3-14)$$

$$\prod_{p=n}^{m-1} N_p = 2^{m-n} (z_0)^{(m-n)/2} \Omega_{\max} \quad (3-15)$$

Solving equation (3-15) will yield an estimate of  $N_p$  and then of the structural index  $N$ , using equation (3-3). In the next sections we will show examples for the application of this method.

### 3.4 Noise and non-linear effects

Finally, we apply the method to the magnetic field of a multisource model (Figure 3.4a): an infinite horizontal line of dipoles with a  $600 \text{ Am}^2$  dipole moment at an  $x_0=305$  m horizontal position and a  $z_0=10$  m depth, and a vertical dyke with  $50 \text{ Am}^2$  dipole moment at an  $x_0=175$  m horizontal position and a  $z_0=20$  m depth. The magnetic inclination is  $60^\circ$  and declination is  $0^\circ$ . The magnetic data are contaminated by addition of independent Gaussian noise, having a zero-mean and a standard deviation of 2% of each datum. We applied the DEXP transformation to the ratio between the second and first-order analytic signal moduli of the anomaly field. First of all, we note that the noise is confined to low altitudes, due to the well-known smoothing effect of the upward continuation operator in the DEXP transformation. We also note at high altitudes a curved part of the rightmost ridge, that is related to the infinite horizontal line of dipoles model (Figure 3.4b). This is due to interference effects, as explained in Appendix B. In addition, we also note that the scaling function is not a straight line (Figure 3.4c), this indicating that with this ratio the problem is non-linear.

As regards the DEXP images, the nonlinear effects due to the interference of the two-source anomalies are evident as a high-intensity “ghost” appears at depth greater than 25 m (Figure 3.4d). Note also that the ghost does not correspond to the horizontal position of any apparent anomaly. So the depth to the top of the dike is well estimated at  $x_0 = 175$  and  $z_0=20$  m with a DEXP value of 0.2248. By using equation (3-15) we obtained a 1.01 structural index. On the other hand, the depth to the centre of the infinitely extended horizontal cylinder is poorly defined because of the nonlinear effects shown by the red circle in Figure 3.4d. This ghost source effect may complicate the whole DEXP section and also the identification of the extreme point of the DEXP image. Due to this we poorly estimate the local maximum point at

$x_0=303$  m and  $z_0=11.6$  m, with a value of  $0.4845 \text{ m}^{-0.5}$ . By using equation (3-15), we estimated a 2.3 structural index, which is higher than the true value ( $N=2$ ).

Such types of non-linearity effects are common to the local wavenumber methods and to other methods based on the analytic signal and horizontal gradient magnitude (e.g., Keating 2009). In the case of the DEXP transformation, we have that while the DEXP of a multisource field is a linear function of the effects of the single sources, this is not so for the DEXP transformation of the ratio, which loses linearity because the ratio  $\mathcal{R}_{mn}$  is in this case:

$$\mathcal{R}_{mn} = \frac{f_{m1} + \dots + f_{mT}}{f_{n1} + \dots + f_{nT}} \quad (3-16)$$

where  $T$  indicates the number of sources. However, linearity may be approximately acquired, in our case, if we meet the conditions that the sources are far enough from each other and/or the order  $n$  of differentiation is enough high that we may write, locally:

$$\mathcal{R}_{mn}(P) \cong \frac{f_{m1} + \dots + f_{mT}}{f_{ni}} \quad i = 1, \dots, T \quad (3-17)$$

where  $P$  indicates points  $P(x,y)$  around the horizontal positions of each source  $P(x_i, y_i)$ .

Let us now describe how the non-linear effect may be made negligible. The key is to consider higher-order derivatives in such a way that the interference effects could be reduced. To prove this we applied the DEXP transformation to the ratio  $\mathcal{R}_{32}$  of the third and second-order analytic signal moduli. Figures 3.4e and 3.4f show that the ridge is now a straight line (Figure 3.4e), as well as the scaling function (Figure 3.4f). Furthermore, the ghost disappears in the DEXP image of  $\mathcal{R}_{32}$  (Figure 3.4g). We estimated the position of the first source at  $x_0 = 175$  m and  $z_0 = 20$  m with a 0.3356 DEXP value giving an  $N=1$  structural index. For the second source, we estimated the position of the source at  $x_0 = 305$  m and  $z_0 = 10.2$  m with a 0.6347 DEXP value giving an  $N= 2.05$  structural index. We conclude that the DEXP of  $\mathcal{R}_{32}$

has enough resolution to make the inherent nonlinearity of the problem negligible and that we may now safely estimate the depth to the two sources. Note that this result was possible because of the high-resolution property of the DEXP transformation, which is stable no matter the order of the differentiation (Cella et al., 2009; Florio et al, 2009). For complex sources, it is recommended to use small values of the difference  $m-n$ , to make the ratio analysis coherent.

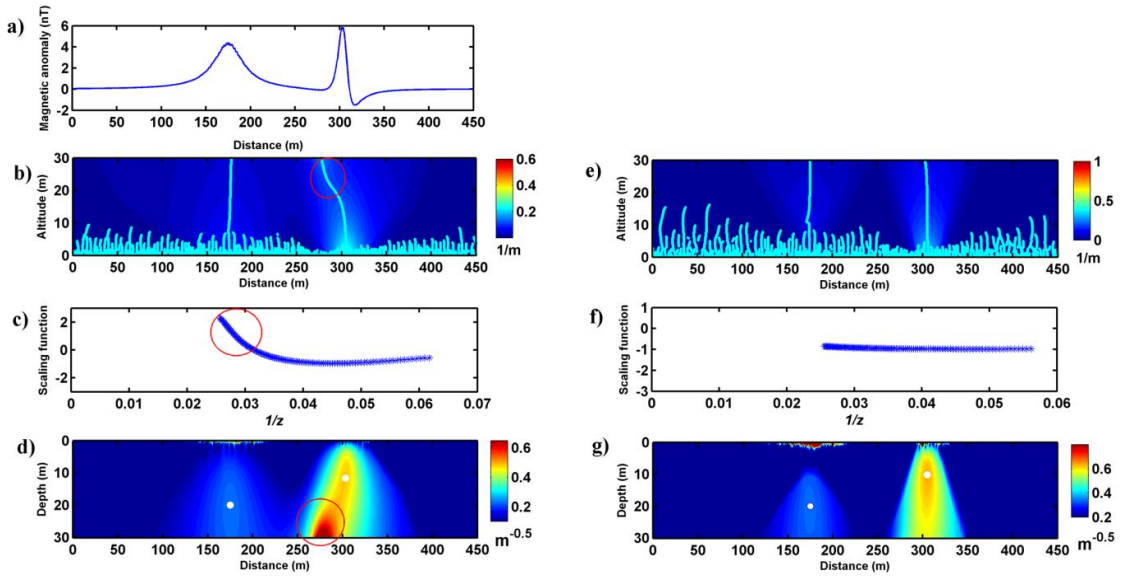


Figure 3.4: Non linearity effects for the automatic DEXP transformation of a multisource model (horizontal cylinder and dike). (a) total field magnetic anomaly profile. The ratio  $\mathcal{R}_{21}$  shows effects of non-linearity at higher altitudes (b), as evidenced within the red circle around the rightmost ridge (cyan solid lines). Same effects occur in the corresponding scaling function along the rightmost ridge (c) and in the DEXP image of the ratio  $\mathcal{R}_{21}$  (d). The picture is completely different in case  $\mathcal{R}_{32}$ : the effects of non linearity are removed as it is clear from the ratio at different altitudes (e), the scaling function along the rightmost ridge (f) and the DEXP image of the ratio  $\mathcal{R}_{32}$  (g). The white dots are at the DEXP maxima, corresponding to the estimated depth to the two sources.

### 3.5 Field Examples

Here we apply the automatic DEXP method to the vertical magnetic anomaly from the Pima copper mine, Arizona, USA. This anomaly is due to a thin dike located at a 64 m depth, as known from drilling information (Gay 1963). The profile was digitized with a 10 m step (Figure 3.5a). We computed the ratio  $\mathcal{R}_{21}$  between the second-order ( $m=2$ ) and first-order ( $n=1$ ) analytic signal moduli of the vertical magnetic anomaly at different altitudes, up to  $z=150$  m, with a 1 m step. Its DEXP image is shown in Figure 3.5b. We find the extreme point at  $x_0=380$  m and  $z_0=64$  m, in good agreement with the known drilling depth. Using equation (3-13), we get  $N_1=1.91$ , that is the structural index is  $N=0.91$ , indicating, approximately, a thin dike model.

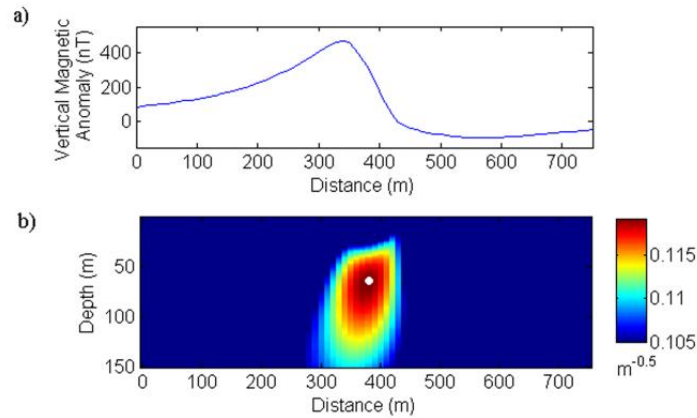


Figure 3.5: The automatic DEXP transformation applied to the magnetic anomaly (vertical component) from the Pima copper mine, Arizona, USA. (a) magnetic anomaly profile and (b) The DEXP image of the ratio  $\mathcal{R}_{21}$ . The white dot is at the DEXP maximum, corresponding to the depth to the source in agreement with known information.

In the second example we analyzed aeromagnetic data (Figure 3.6a) measured during a high-resolution survey over the Hamrawien area, along the western margin of the Red Sea, Egypt (Salem et al. 2005). The flight lines were directed N60E and the average terrain

clearance was 150 m, with a sampling interval of approximately 10 m. We digitized the data from figure 3a of Salem et al. (2005) with a sampling step of 10 m. The data have two high-amplitude anomalies that were interpreted as diabase dykes associated with the Red Sea rifting (Salem et al. 2005). These two anomalies were interpreted by the Enhanced Local Wavenumber method (Salem et al., 2005), the AN-EUL method (Salem and Ravat, 2003) and multi-deconvolution analysis (Salem, 2011) and the results indicated for both sources a structural index  $N$  between 1.17–1.6, and depths between 422–600 m below the magnetic sensor. More recently, Florio and Fedi (2014) interpreted the same data with the multiridge Euler deconvolution method and obtained for the two sources depth estimates between 400 and 430 m, corresponding to structural indices of 1.05-1.1.

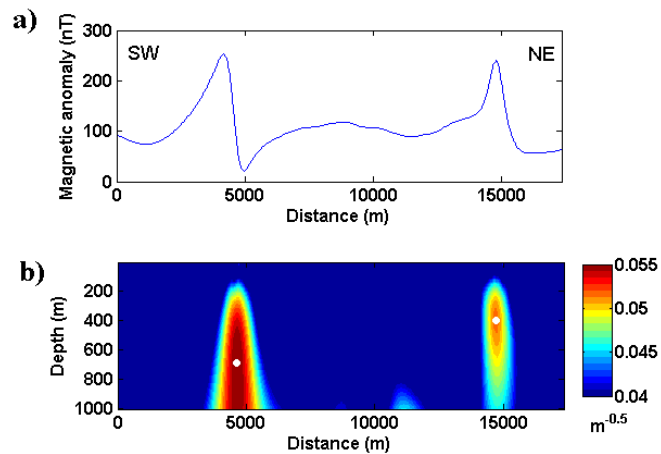


Figure 3.6: The automatic DEXP transformation applied to the aeromagnetic anomaly over the Hamrawien area, Egypt. (a) magnetic anomaly profile and (b) The DEXP image of the ratio  $\mathcal{R}_{21}$ . The white dots are at the DEXP maxima, corresponding to the depth to the sources.

We applied the DEXP transformation to the ratio  $\mathcal{R}_{21}$  between the second- and first-order analytic signal moduli of the aeromagnetic line. The DEXP image (Figure 3.6b) shows a 690 m depth at a  $0.05521 \text{ m}^{-0.5}$  DEXP extreme point for the south-western source giving a 1.9 structural index, indicating a depth to the centre of the source. In the case of the north-eastern

source, the DEXP image shows a 400 m depth at a  $0.0516 \text{ m}^{-0.5}$  DEXP extreme point giving a 1.06 structural index indicating a depth to the top of the source.

Finally we applied the method to a magnetic survey carried out for iron exploration in Cataldere, Bala district of Turkey. The surface of the area is entirely covered by an alluvial horizon with a thickness of 2–3 m and the topography is rather flat. The few small outcropping magnetite blocks in the skarn zone appear in a very small part of the area, east of the drill-hole C1 (Aydin, 2008).

The magnetic total field intensity measurements were acquired using a proton magnetometer with an accuracy of 1 nT; they have varying intervals from 2 m to 10 m along profiles spaced at 20 m, because the density of the measurement stations was increased in the places where the magnetic gradient was high. Figure 3.7a shows the magnetic anomaly map with the drilling locations and the depths to the ore projected along a profile AA' (modified after Aydin, 2008). The magnetic map is digitized with a 2 m horizontal step (Figure 3.7a). Figure 3.7b shows the available information from drillings, showing that the biggest thickness of the ore is at the middle part of the map (boreholes C1 and CD1), while it decreases at borehole C3 and is negligible at boreholes C2 and CD7.

The DEXP transformation is applied to the ratio  $\mathcal{R}_{21}$  of the total gradient with a 2 m step along  $z$ -axis and a 10 % stabilization. Figure 3.8 shows two slices of the DEXP transformed volume passing through the causative source. The extreme value of the DEXP slices at a depth of 62 m corresponds to the causative source depth. The DEXP result agrees well with the drilling information shown in Figure 3.8b in boreholes C2 and CD7.

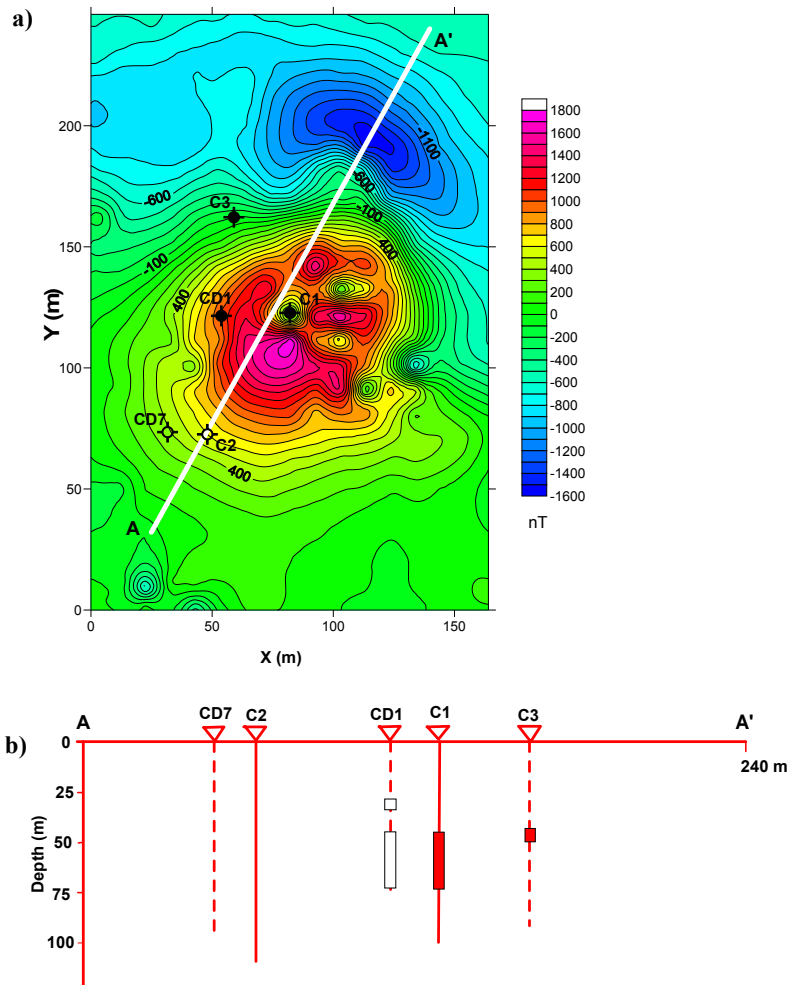


Figure 3.7: a) The magnetic contour map of a survey in Cataldere, Bala district of Turkey and the locations of boreholes and b) boreholes drilling depths to the ore along the profile AA' (modified after Aydin, 2008). Solid lines indicate the boreholes along the profile and dashed lines indicate a projection of boreholes on the profile.

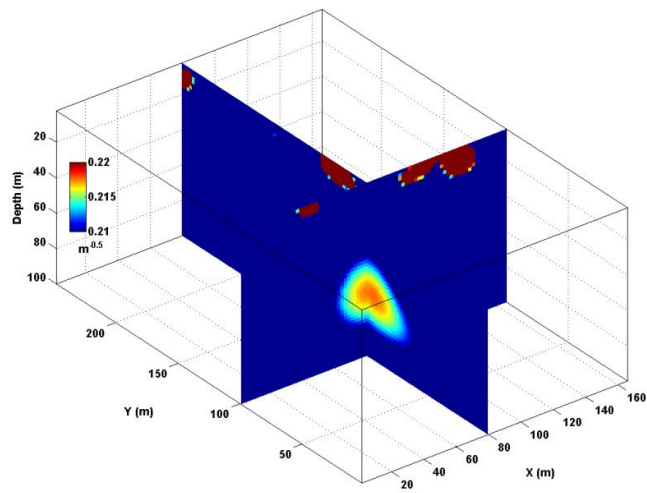


Figure 3.8: The 3D automatic-DEXP transformed field. Two Slices of the DEXP transformed volume with extreme point at  $z=62$  m. Note that the noise is restricted to the low altitudes.

## ***Chapter 4***

### ***Improving the local wavenumber method by automatic DEXP transformation***

*This chapter is published as: [Abbas, M. A.](#), Fedi, M., and Florio, G., 2014, Improving the local wavenumber method by automatic DEXP transformation. *Journal of Applied Geophysics*, 111, 250-255.*

#### **4.1 Introduction**

In the last decades some semi-automated methods were developed to perform a fast interpretation of potential fields. These methods help recovering the horizontal position, the depth and the structural index of ideal simple sources approximating the true geologic structures. The structural index  $N$  is an integer defining the source shape and varies from 0 to 3 in the magnetic case (Thompson, 1982). Among these semi-automated methods, the local wavenumber (LWN) is widely known (Thurston and Smith, 1997). The LWN function is defined as the horizontal derivative of the local phase, its computation involving second-order spatial derivatives. The LWN method has evolved as a multi-model technique (Smith et al., 1998), able to provide depth and structural index estimates for any 2D source. However, due to the use of the second-order local wavenumber, it involves computation of third-order derivatives of the field. A further enhancement of the LWN method uses the local-wavenumber and its phase-rotated version, so allowing the estimation of the 2D source parameters using derivatives up to the second order (Salem et al., 2005). Later, Salem et al. (2008) derived a 3D Euler equation using the derivatives of the tilt angle, a quantity very similar to the local phase. This method relies on second-order derivatives of the field and can provide depth and structural index estimates. Finally, Keating (2009) devised one more method to estimate the source parameters from the vertical derivative of the LWN, based on

the computation of the local wavenumber at different altitudes and applying a finite-difference algorithm. A 3D formulation of LWN was also given by Phillips et al. (2007).

As can be appreciated from this brief presentation of methods based on the LWN, a very important issue, often limiting the practical application of this class of methods, regards the noise amplification due to the use of high-order derivatives. To circumvent this effect, we present a new multiscale method, which is highly stable vs. high wavenumber noise. In particular, we will consider the DEXP transformation (Fedi, 2007, Fedi and Abbas 2013) of the LWN and will derive a simple scaling-law, which is specific for this function.

The DEXP transformation of potential fields is very stable (Fedi, 2007; Fedi and Pilkington, 2012; Fedi and Florio, 2013), thanks to its composite upward continuation-vertical derivative operator, which behaves as a band-pass filter (Cella et al., 2009; Florio et al., 2009). As a very attractive feature, the DEXP transformation of the LWN may be fully automated, so to be implemented as a fast imaging method, mapping every source at the correct depth.

We finally recall that LWN is a nonlinear function of the potential fields of interfering sources. We will show that the above-mentioned stability of the Local Wavenumber DEXP transformation in handling with high-order field derivatives, may be used as an effective tool to control the effects of non-linearity.

## 4.2 Theory

Let us assume a Cartesian coordinate system where  $x$  and  $z$  are the horizontal and vertical directions respectively and the depth is positive downward., the first-order local wavenumber  $k_1$  of a potential field,  $f$ , for 2D sources is defined as the rate of change of the local phase of the analytic signal (Bracewell, 1965):

$$k_1 = \frac{\partial}{\partial x} \tan^{-1} \left( \frac{\partial f / \partial z}{\partial f / \partial x} \right) \quad (4-1)$$

Thurston and Smith, 1997, showed that  $k_1$  could be written as

$$k_1 = \frac{1}{|A(x)|^2} \left( \frac{\partial^2 f}{\partial x \partial z} \frac{\partial f}{\partial x} - \frac{\partial^2 f}{\partial x^2} \frac{\partial f}{\partial z} \right) \quad (4-2)$$

where

$$|A| = \left[ \left( \frac{\partial f}{\partial x} \right)^2 + \left( \frac{\partial f}{\partial z} \right)^2 \right]^{1/2} \quad (4-3)$$

is the 2D modulus of the analytic signal  $A$  (Nabighian, 1972).

The local wavenumber of the magnetic field of a 2D source at a horizontal position  $x_0$  and a depth  $z_0$ , can be written as (Smith et al., 1998):

$$k_1(x, z) = - \frac{(N+1)(z-z_0)}{(x-x_0)^2 + (z-z_0)^2} \quad (4-4)$$

where  $N$  is the structural index, a quantity related to the source geometry (Thompson, 1982), assuming, in the magnetic case, the integer values 0, 1, 2 for contact, dyke and horizontal cylinder models, respectively.

The second-order local wavenumber can be written as (Smith et al., 1998):

$$k_2(x, z) = \frac{\partial}{\partial x} \tan^{-1} \left( \frac{\partial^2 f / \partial z^2}{\partial^2 f / \partial x \partial z} \right) = - \frac{(N+2)(z-z_0)}{(x-x_0)^2 + (z-z_0)^2} \quad (4-5)$$

We can generalize equations (4-4) and (4-5) for any higher order of the local wavenumber of the potential field as:

$$k_p(x, z) = \frac{\partial}{\partial x} \tan^{-1} \left( \frac{\partial^p f / \partial z^p}{\partial^p f / \partial x \partial z^{p-1}} \right) = - \frac{N_p(z-z_0)}{(x-x_0)^2 + (z-z_0)^2} \quad (4-6)$$

where  $p$  is the order of the local wavenumber and  $N_p = N+p$ .

We now recall the main theoretical aspects of the DEXP transformation (Fedi, 2007) and apply it to the local wavenumber function. The key concept of the DEXP theory is the scaling

function  $\tau$ , defined as the derivative of the logarithm of the potential field,  $f$ , or of any of its partial derivatives of order  $p$ ,  $f_p$ , with respect to  $\log(z)$  (Fedi, 2007). Along any line defined by the zeros of the horizontal derivatives of  $f_p$ ,  $\tau$  assumes the simple expression:

$$\tau = \frac{\partial \log(f_p)}{\partial \log(z)} = -N_p \frac{z}{z - z_0} \quad (4-7)$$

Similarly, we may compute now the scaling function of the local wavenumber  $k_p$ . Using equation (4-6), we so obtain:

$$\tau(k_p) = \frac{\partial \log(k_p)}{\partial \log(z)} = -\frac{z}{z - z_0} \quad (4-8)$$

Equation (4-8) shows that  $\tau(k_p)$  is, differently from  $\tau(f_p)$ , independent of  $N$ .

Again following the approach by Fedi (2007) we note that, at  $z=-z_0$ ,  $\tau=-0.5$ . From this result, it follows that:

$$\left. \frac{\partial \log(k_p)}{\partial z} \right|_{z=-z_0} = -0.5 \left. \frac{\partial \log(z)}{\partial z} \right|_{z=-z_0} \quad (4-9)$$

or

$$\left. \frac{\partial [\log(k_p) + 0.5 \log(z)]}{\partial z} \right|_{z=-z_0} = 0 \quad (4-10).$$

So, the function  $\log(k_p) + 0.5 \log(z)$  has an extreme point at  $z=-z_0$ . Consequently, we have also that:

$$\left. \frac{\partial (z^{0.5} k_p)}{\partial z} \right|_{z=-z_0} = 0 \quad (4-11).$$

From this equation, we may finally obtain the formula for the DEXP transformation of the local wavenumber of  $p$ -order:

$$\Omega_p = z^{0.5} k_p \quad (4-12)$$

which shows that Local Wavenumber DEXP has an extreme point at  $z=-z_0$ , i.e. at the altitude equals to the opposite of the depth to the source. This is similar to the DEXP transformation

of potential fields (Fedi, 2007), but has the advantage of not depending on the preventive determination of the structural index,  $N_p$ .

However, we may easily estimate also  $N_p$ , at the local wavenumber DEXP maxima  $\Omega_{\max}$ . In fact, using equations (4-6) and (4-12), at the points  $(x, z) = (x_{\theta}, z_{\theta})$  we find:

$$N = 2z_0^{0.5} \Omega_{\max} - p \quad (4-13)$$

The method can be extended to the 3D case by using the appropriate formulation of the local wavenumber (Phillips et al., 2007).

We conclude that, differently from the DEXP transformation of potential fields, the DEXP transformation of the local wavenumber  $k_p$  yields the depth to the source, independent of the structural index. This is a major improvement on the original theory, because sources of different  $N$  may be now automatically imaged at the correct depth in the same section.

### 4.3 Synthetic Examples

We test the method analyzing the magnetic field of three different kinds of sources: a magnetic contact with a 0.05 A/m magnetization at the position  $(x_0, z_0) = (75, 10)$  m, a vertical dyke with a 1 A/m magnetization at the position  $(x_0, z_0) = (150, 5)$  m and an infinite horizontal dipole-line with a 4 A/m magnetization at the position  $(x_0, z_0) = (225, 5)$  m. The magnetic inclination and declination are  $56^\circ$  and  $2^\circ$ , respectively.

The magnetic data profile (Figure 4.1a) is sampled at 0.25 m step and the local wavenumber is computed at altitudes from 0 to 20 m with a 0.1 m step. The first-order local wavenumber  $k_1$  at the ground level ( $z=0$ ) is computed using equation (4-1) and it is shown in Figure 4.1b. Here we assume that we know the exact values of the structural indices of the three causative sources, and we used these values to calculate the depth to the sources by the standard approach of Smith et al. (1998) using equation (4-4). The local peak values of  $k_1$

corresponding to the three sources are  $0.09128 \text{ m}^{-1}$ ,  $0.3634 \text{ m}^{-1}$  and  $0.5137 \text{ m}^{-1}$  for the magnetic contact, dyke and cylinder, respectively, and the corresponding depth estimates are 10.96 m, 5.5 m and 5.48 m. The error in the depth estimation could be related to the interference effect.

Let us now apply the DEXP transformation (equation 4-12) to the local wavenumber, after having computed it at different altitudes. We obtain the DEXP image shown in Figure 4.1c. From this image, using the extreme values, we can estimate a 10 m depth to the magnetic contact source at a horizontal position of 75 m with a  $0.1598 \text{ m}^{-0.5}$  local wavenumber DEXP value, yielding a structural index of  $N=0.01$ . This result agrees well with the known parameters of the model. In the area of the other two sources, the local wavenumber DEXP section displays two couples of strong highs and lows (highlighted by the two dashed circles in Figure 4.1c). These features, clearly not usable for any depth estimation, are interpretable as the effect of interference. This kind of feature is actually well known (e.g., Keating, 2009) and is due to the inherent nonlinearity of the local wavenumber function. Interestingly, it results very easy to identify these spurious features in the DEXP section, because these localized bipolar behaviour in the interference area cannot be related to any real source. To reduce the interference effect and to increase the resolution of the DEXP image, we can however use a higher-order local wavenumber, since, as already said, the DEXP transformation is very stable vs. the differentiation order. Here we calculated the second-order local wavenumber, as shown in Figure 4.1d, and the DEXP transformation was applied to the local wavenumber computed at different altitudes (Figure 4.1e). In this way, the resolution of the DEXP image is improved and the effect of the interference is reduced; the bipolar feature can be seen only in a shallow part of the image at a horizontal position  $x=200 \text{ m}$  as indicated by the dashed circle in Figure 4.1e. From the extreme points of the DEXP image, we obtained correctly the depth to the three sources as 10 m, 5 m and 5 m for the magnetic contact, dyke and horizontal cylinder, respectively. The values of the DEXP image at the extreme points are

0.3157  $\text{m}^{-0.5}$ , 0.6758  $\text{m}^{-0.5}$  and 0.8962  $\text{m}^{-0.5}$ , yielding estimated structural indices equal 0, 1.02 and 2.01, so well corresponding to those of magnetic contact, dyke and horizontal cylinder, respectively. These results agree with the known parameters of the models.

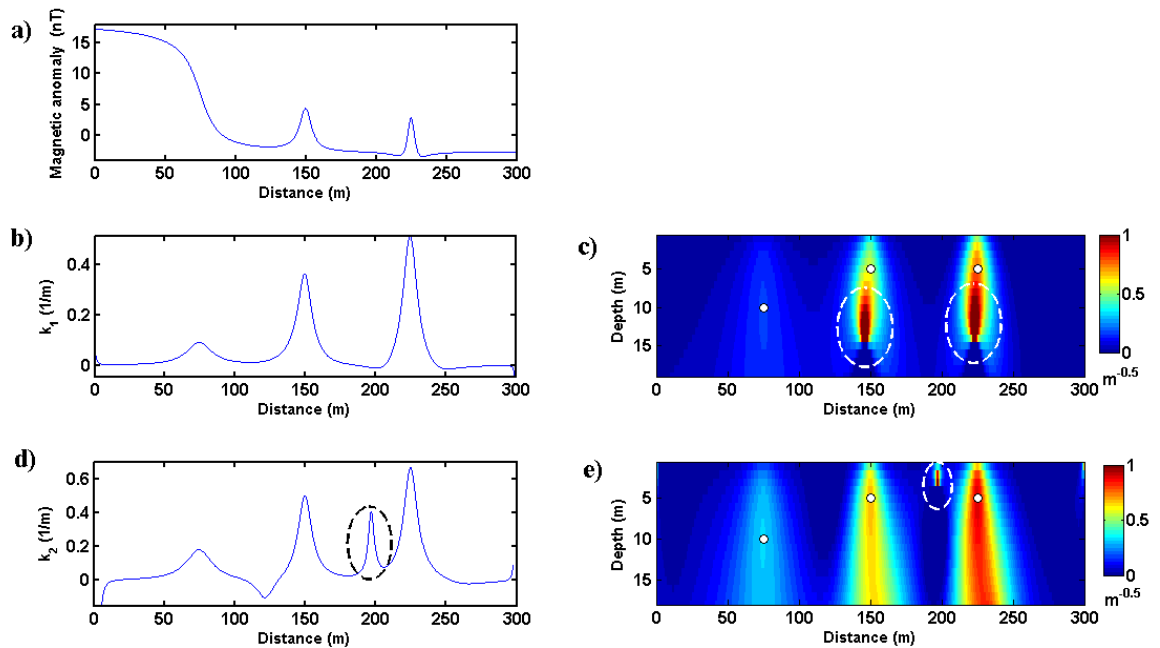


Figure 4.1: The DEXP transformation applied to the local wavenumber of the noise-free magnetic field of a contact (leftmost), a vertical dike (middle) and a horizontal cylinder (rightmost). (a) The magnetic anomaly profile, (b) the first-order local wavenumber computed at the ground level, (c) the DEXP image obtained from the first-order local wavenumber, (d) the second-order local wavenumber computed at the ground level and (e) the DEXP image obtained from the second-order local wavenumber. The white points in the DEXP images in c) and e) indicate the sources' locations whereas the dashed circles in c), d) and e) highlight the nonlinear effects.

In the second example we contaminated the previous model data with addition of independent Gaussian noise having a zero mean and a standard deviation of 1% of each datum (Figure 4.2a). In Figure 4.2b the first-order local wavenumber  $k_1$  at the ground level is shown. It is evident the strong enhancement of the noise that makes it almost impossible to recognize

any features related to the original signal. On the other hand, in the DEXP image (Figure 4.2c), the noise is confined to the shallowest scales and the signal at deeper levels is preserved, allowing good depth and structural index estimates to be obtained. The depth to the contact model is well defined by the DEXP extreme point at  $(x, -z) = (75 \text{ m}, 10 \text{ m})$  at which the value of the scaled local wavenumber DEXP equals  $0.1596 \text{ m}^{-0.5}$ . By substitution of this value in equation (4-13), we estimated the structural index as  $N=0.01$  which agrees with the theoretical structural index of a magnetic contact. As in the noise-free case (Figure 4.1c) it is possible to note in Figure 4.2c the presence of a localized bipolar behaviour in correspondence of the other two sources, at  $x=146 \text{ m}$  and  $x = 223 \text{ m}$ , preventing any reliable depth estimation. So, similarly to the previous case, we calculated the DEXP of the second-order local wavenumber  $k_2$  (Figure 4.2d) and from this we obtained the local wavenumber DEXP image in Figure 4.2e. Again, the noise results confined to the shallowest scales in this DEXP image, while the local wavenumber at the ground level (Figure 4.2d) is overwhelmed by noise. Once more, we highlight as multiscale methods such as DEXP are inherently stable and the use of high-order derivatives does not imply, at most scales, a deterioration of the signal-to-noise ratio. On the other hand, high-order derivatives allow the resolution of the DEXP image to be increased, reducing the nonlinearity effects. It is easy to see that the maxima of the DEXP image in Figure 4.2e are at the correct depth for each of the three different sources, even though the sources have different structural indices. We found a  $0.32 \text{ m}^{-0.5}$  maximum at  $(x, -z) = (74.8 \text{ m}, 10 \text{ m})$ , a  $0.68 \text{ m}^{-0.5}$  maximum at  $(x, -z) = (150 \text{ m}, 5.2 \text{ m})$  and a  $0.89 \text{ m}^{-0.5}$  maximum at  $(x, -z) = (225 \text{ m}, 5 \text{ m})$ . These depth and horizontal position estimates are then used in equation (4-13) to obtain the structural index for each source. The obtained values for  $N$  are:  $N=0$ ,  $N=1.08$ , and  $N=2.01$ , respectively, so indicating a contact, a dike and a horizontal cylinder model. These results agree well with the theoretical structural indices of the three sources.

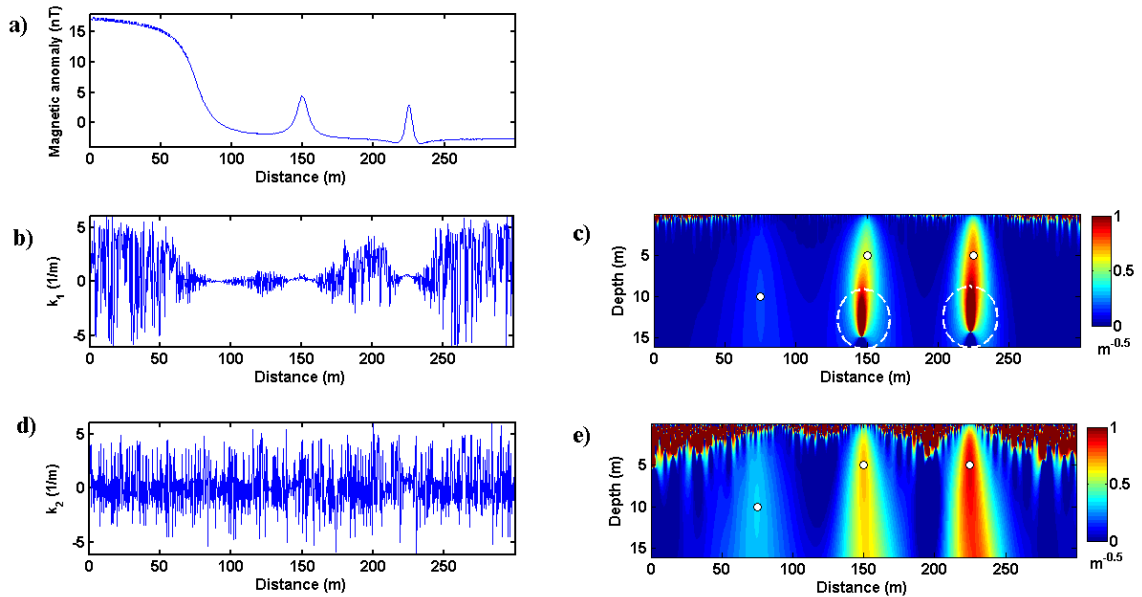


Figure 4.2: The DEXP transformation applied to the local wavenumber of the noisy magnetic field of a contact (leftmost), a vertical dike (middle) and a horizontal cylinder (rightmost). (a) The magnetic anomaly profile, (b) the first-order local wavenumber computed at the ground level, (c) the DEXP image obtained from the first-order local wavenumber, (d) the second-order local wavenumber computed at the ground level and e) the DEXP image obtained from the second-order local wavenumber. The white points in the DEXP images in c) and e) indicate the sources' location whereas the dashed circles in c) highlight the nonlinearity effect.

Finally, we applied the method to the magnetic field of a prism with a 10 m depth to the top, a 100 m depth to the bottom and a 1 A/m magnetization. The inclination and declination of the magnetic field are  $90^\circ$  and  $0^\circ$ , respectively. The magnetic data map, sampled with a 1 m step, is shown in Figure 4.3a. We applied the DEXP transformation to the first-order local wavenumber computed at different altitudes and we obtained the DEXP volume shown in Figure 4.3b. First we note that the local wavenumber DEXP well points out the depth to the top of the prism, which is well assessed all around its boundary, at the correct depth. This is clearly indicated by the highest values of the local wavenumber DEXP occurring at 10 m

depth. Once again we note that this fine estimate is automatically determined, since the local wavenumber DEXP is independent of the structural index value.

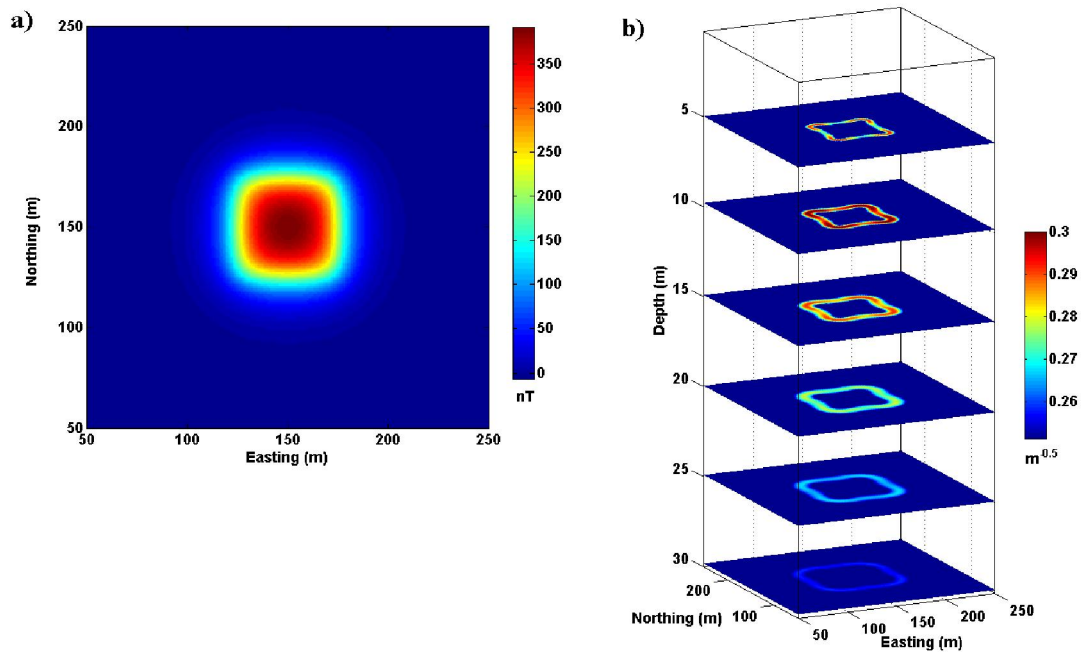


Figure 4.3: The DEXP transformation applied to the first-order local wavenumber of the magnetic field of a prism model. a) The magnetic anomaly map, and (b) horizontal slices of the DEXP volume computed from the first-order local wavenumber. The DEXP transformation images correctly the top of the prism at the appropriate depth at 10 m all around its boundaries.

## 4.4 Field Examples

### 4.4.1 Known Source: test site, Central Italy

As a first real case, we applied our method to the magnetic vertical gradient anomaly of a group of buried drums in a test site set-up to study the magnetic signature of metallic objects in the Apennines, Central Italy (Marchetti et al., 1998). The site is characterized by fluvial-glacial deposits consisting of conglomerate in a silt-sandy matrix, with very low magnetic properties (Marchetti et al., 1998).

A group of 12, 55-gallon, new steel drums were vertically oriented, and buried at 4.5 m depth. The entire buried body had the rough shape of a prism 88 cm thick, having a 2x3 m base with its longer side E-W oriented. A magnetic gradiometry survey was carried out in the site with a proton precession magnetometer in an area of 22m x 25 m. The distances to the ground level of the bottom and top sensors were 75 cm and 150 cm respectively. The survey was carried out along profiles spaced 1 m each other at a sampling interval of 1 m. The vertical gradient ranges between -18 nT/m and 23 nT/m (Marchetti et al., 1998). We carefully digitized these data from figure 4 of Marchetti et al.(1998).

We upward continued the vertical gradient at a range of altitudes from 0 to 10 m with a 0.2 m vertical step and we computed their second-order local wavenumber  $k_2$  (Figure 4.4a). Then, we applied the DEXP transformation by using equation (4-12) and two vertical sections of the DEXP volume are plotted in Figure (4.4b,c) to image the distribution of the causative sources in the subsurface. Because of the ratio between the depth to the drums and their thickness is sufficiently big, the drums can be seen as a unique body in the DEXP volume. The found depth is 4.5 m after subtracting the average sensor altitude (1.12 m), perfectly consistent with the true burial depth, and the estimated structural index is 2.6. In both sections the noise is confined at the shallow altitudes.

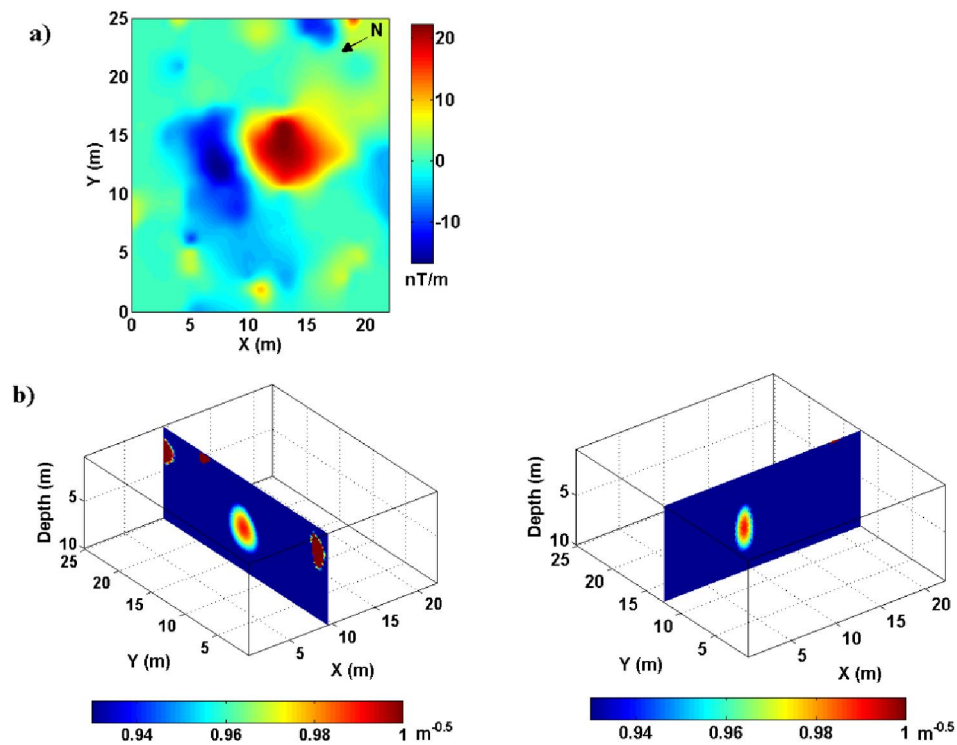


Figure 4.4: The DEXP transformation applied to the local wavenumber of the magnetic vertical gradient field over buried drums in a test site in central Italy. (a) The magnetic vertical gradient anomaly map; and (b) two vertical slices along the DEXP volume computed from the second-order local wavenumber.

#### 4.4.2 Unknown source: southeast Bulgarian Black Sea shelf

We analyzed a profile perpendicular to an elongated anomaly from the southeast Bulgarian Sea shelf (Gerovska et al., 2009; Stavrev et al., 2009). The area is characterized by magnetic anomalies related to Upper Cretaceous volcanic and plutonic structures. The reverse magnetization is dominant in the area. The profile was carefully digitized from Stavrev et al. (2009, figure 6) with a 0.01 km horizontal step (Figure 4.5a). The DEXP transformation was applied to the first-order LWN calculated at different altitudes. The local wavenumber DEXP (Figure 4.5b) shows an extreme point at a 3 km depth. At the extreme point we also estimated a 1.56 structural index. Stavrev et al. (2009) interpreted this anomaly using differential similarity transforms and estimated very similar source parameters (2.8 km depth and  $N=1.7$ ).

However, with respect to their method, involving the search for the position of a central similarity point for tentative structural indices, the application of our method is easier for both depth and structural index.

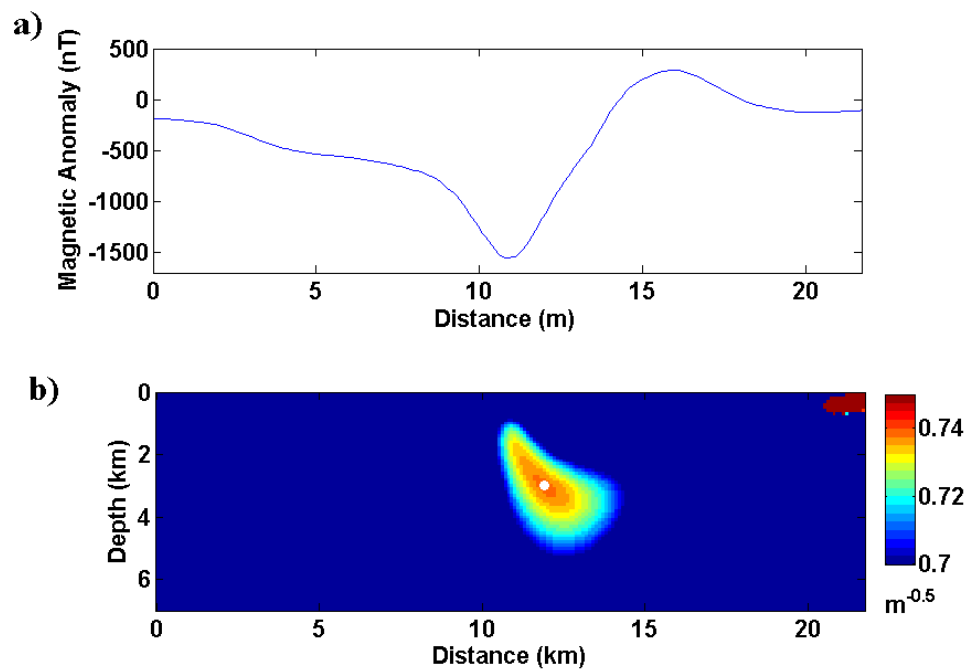


Figure 4.5: The DEXP transformation applied to the local wavenumber of a magnetic profile from southeast Bulgarian Sea shelf. a) The magnetic anomaly profile; b) The DEXP image computed from the first-order local wavenumber. The white point indicate the estimated depth to the source.

## ***Chapter 5***

### ***Fractional-order local wavenumber: an improved source-parameter estimator***

*(accepted as a poster presentation at the 77th EAGE Conference & Exhibition, Madrid, 2015).*

#### **5.1 Introduction**

As it was mentioned in the previous chapter the main factor limiting the use of the local wavenumber methods in the interpretation of potential field data is the amplification of noise effect in the data due to the use of high-order derivatives in their computations. In this chapter we propose to use a local wavenumber based on fractional-order field derivatives. We will show that a fractional-order local wavenumber allows noise reduction and improved depth and structural index estimates. As regards the application of the fractional-order differentiation to potential fields, Gunn et al. (1997) noticed the use of fractional-order vertical derivatives, such as those of order 0.5, 1.5, to the end of reducing the noise amplification. Cooper and Cowan (2003) showed that the use of the fractional-order gradients of potential field data enhanced the analytic signal and Euler deconvolution techniques. Phillips et al. (2007) used a half-order vertical integral of magnetic data in the application of the total gradient (analytic signal magnitude) method to estimate the depth to the sources.

#### **5.2 Theory**

If we consider the potential field  $f$  of 2D sources and its directional derivatives in  $x$ - and  $z$ -directions in Cartesian coordinates, the first-order local wavenumber  $k_1$  is defined by Thurston and Smith (1997) as:

$$k_1 = \frac{\partial}{\partial x} \tan^{-1} \left( \frac{\partial f / \partial z}{\partial f / \partial x} \right) \quad (5-1)$$

In cases of magnetic contact, thin sheet and horizontal cylinder,  $k_1$  was shown by Smith et al. (1998) to be equal to:

$$k_1 = \frac{(N+1)z_0}{(x-x_0)^2 + z_0^2} \quad (5-2),$$

where  $x_0$  is the source horizontal location,  $z_0$  is the depth to the source and  $N$  is the structural index of the source, respectively equal to 0, 1, and 2 for magnetic contact, thin sheet and horizontal cylinder (Thompson, 1982).

Similarly, Smith et al. (1998) showed that the second-order local wavenumber,  $k_2$ ,

$$k_2 = \frac{\partial}{\partial x} \tan^{-1} \left( \frac{\partial^2 f}{\partial z^2} / \frac{\partial^2 f}{\partial x \partial z} \right) \quad (5-3)$$

may be defined as:

$$k_2 = \frac{(N+2)z_0}{(x-x_0)^2 + z_0^2} \quad (5-4).$$

To reduce the LWN noise amplification involved by high-order derivatives, we here propose to define the local wavenumber on the basis of fractional-order field derivatives instead than integer-order derivatives.

To this end, we first generalize equations 5-1, 5-2, 5-3 and 5-4 for any real  $p$ -order derivative of the field:

$$k_p = \frac{\partial}{\partial x} \tan^{-1} \left( \frac{\partial^p f}{\partial z^p} / \frac{\partial^p f}{\partial x \partial z^{p-1}} \right) \quad (5-5)$$

Note that when  $p < 1$ , this means that the local wavenumber is calculated from a fractional-order derivative of the integral of the field.

The  $p$ -order derivative/integral  $f_p$  of a potential field  $f$  can be calculated in the frequency domain (Gunn, 1975; Cooper and Cowan, 2003) as:

$$F(f_p) = \omega^p F(f) \quad (5-6)$$

where  $F$  is the Fourier transform and  $\omega$  is the wavenumber.

Here, we show that a suitable selection of fractional order  $p$  of the fractional integration-differentiation allows a local wavenumber formulation which is more convenient than that based on the standard integer-order differentiation. To this end, let us first assume that:

$$k_p = \frac{(N+p)z_0}{(x-x_0)^2 + z_0^2} \quad (5-7).$$

Even though we do not demonstrate theoretically equation (5-7), we found numerically that it holds on for ideal source models such as cylinder, dyke and contact (see appendix C). Considering the iSPI<sup>TM</sup> method of Smith et al. (1998). They presented a model-independent local wavenumber calculated as  $(k_2 - k_1)$ , where integer orders field derivatives are used.

Using equation (5-7), we here generalize the formula for any two *real* orders of differentiation/integration of the field ( $p_1$  and  $p_2$ ) as:

$$k_{p_1} - k_{p_2} = \frac{(p_1 - p_2)z_0}{(x-x_0)^2 + z_0^2} \quad (5-8).$$

The depth to the source can be estimated at the maximum point ( $x=x_0$ ) as

$$z_0 = \frac{p_2 - p_1}{k_{p_2} - k_{p_1}} \quad (5-9).$$

and the structural index  $N$  can be estimated as

$$N = k_{p_1} \frac{p_2 - p_1}{k_{p_2} - k_{p_1}} - p_1 \quad (5-10).$$

Finally we can apply the local wavenumber DEXP imaging (LWN-DEXP) method of Abbas et al. (2014) to the fractional-order LWN. The DEXP transformation  $\Omega_p$ , in case of the local wavenumber DEXP imaging, is defined as:

$$\Omega_p = z^{0.5} k_p \quad (5-11)$$

where the depth to the source is estimated from the extreme point of the DEXP image. The structural index  $N$  can be found at the extreme point as:

$$N = 2z_0^{0.5} \Omega_{\max} - p \quad (5-12)$$

where  $p$  is the fractional order of differentiation.

### 5.3 Synthetic Examples

Here we applied the fractional-order LWN method to the magnetic anomaly field of a horizontal cylinder at a 200 m horizontal position and a 10 m depth (Figure 5.1a). The inclination and declination of the magnetic field are  $60^\circ$  and  $0^\circ$ , respectively. The data-step is 1 m. First, to show the validity of the proposed method, we apply a fractional-order local wavenumber DEXP (equation 5-11). We calculate the local wavenumber of the magnetic field of the above-mentioned model considering different orders of LWN  $p= 1.3, 1.8$  and  $2.3$  (Figure 5.1). The estimated depth and structural indices are shown in Table 1. We can note that the results agree with the known parameters of the model despite of using fractional orders of the LWN.

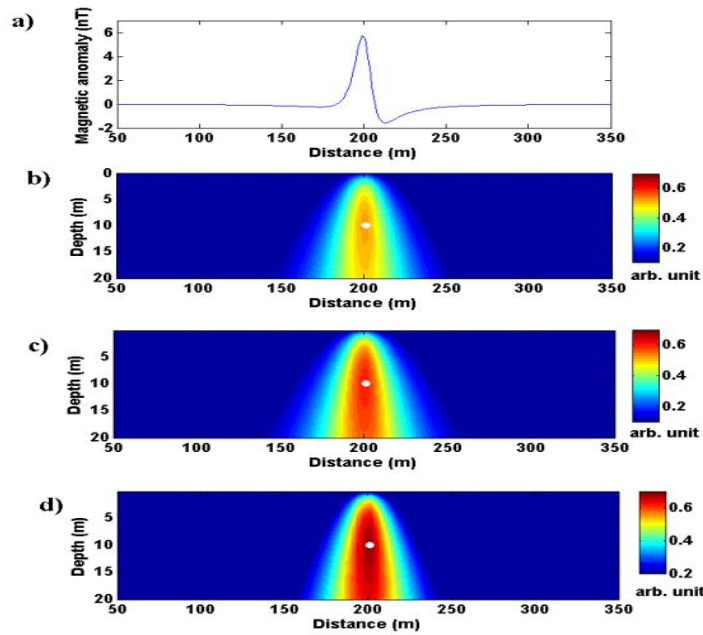


Figure 5.1: Application of the DEXP transformation to fractional-orders LWN. (a) The Magnetic anomaly of a horizontal cylinder model; (b) the DEXP image of the 1.3-order

LWN; (c) the DEXP image of the 1.8-order LWN; and (d) the DEXP image of the 2.3-order LWN. The white points in b), c), and d) indicate the estimated depth to the source.

Table 5.1: The results of the DEXP transformation applied to different fractional-orders LWN.

Order of LWN	DEXP Maximum point $\Omega_{\max}$	Depth $z_0$	Structural index $N$
1.3	0.5191	10	1.98
1.8	0.5983	10	1.98
2.3	0.6773	10	1.98

Now, we apply the fractional-order LWN to the iSPI<sup>TM</sup> method (Smith et al., 1998). We used  $p_1=1.1$  and  $p_2=1.2$  as fractional orders of differentiation (Figure 5.2a, b, d & e). The fractional-order local wavenumber was computed using equations (5-5) and (5-7) as shown in Figure 5.2c & f. Then we calculated the depth and structural index (Figure 5.2h & i) at the peak of  $k_{1.2}-k_{1.1}$  shown in Figure 5.2g, using equations (5-9) and (5-10), as  $z_0=10$  m depth and  $N=2$ . These estimates agree perfectly with the true values of the source parameters.

Finally, we test the method against noise by adding to the magnetic field of the horizontal cylinder a Gaussian noise having a zero-mean and a standard deviation of 2% of each datum. Here we integrated vertically the field one-order and then differentiated it by orders  $p= \{0; 0.1\}$ . Then we calculated the LWNs of the orders  $p_1=0, p_2=0.1$  using equation (5-5), and also the  $k_{0.1}-k_0$  difference (Figure 5.3). We compared our results to that obtained by the iSPI<sup>TM</sup> method (Smith et al., 1998) applied to the vertical integral of the field i.e.,  $k_I-k_0$ , as suggested by Phillips et al. (2007) to reduce the noise amplification. In the fractional-order LWN case, we obtained a 9.88 m depth and an  $N= 1.87$  structural index (Figure 5.3d, e, f).

Besides the fine estimates of the source parameters, we note that the peak of the difference is well evidenced and correspond to the same horizontal position than those of  $k_{0.1}$  and  $k_0$ , so that the application of the method by Smith et al. (1998) is straightforward. Instead, in the integer-order LWN case (Figure 5.3g), we note two areas of apparent peaks (at

horizontal distances, 90 and 293 m) which do not correspond to any peak in  $k_0$  while in the central zone the peak corresponding to the source location may hard be identified. However, referring to the position at horizontal distance 200 m, corresponding to the peak positions in  $k_0$  and  $k_j$ , we can estimate a 7.06 m depth and an  $N= 1.77$  structural index (Figure 5.3h, i). This example shows how the use of fractional-order local wavenumber can improve the classical LWN method.

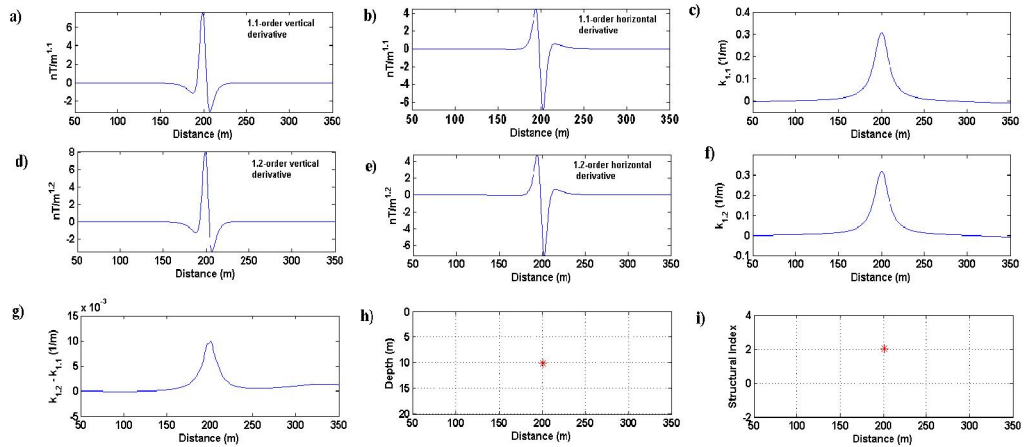


Figure 5.2: Application of the fractional-order local wavenumber to the magnetic field of a horizontal cylinder. a) The 1.1-order vertical derivative of the field; b) the 1.1-order horizontal derivative of the field; c) the 1.1-order local wavenumber; d) the 1.2-order vertical derivative of the field; e) the 1.2-order horizontal derivative; f) the 1.2-order local wavenumber; g) the  $k_{1.2}-k_{1.1}$  local wavenumber; h) the estimated depth to the source and i) the estimated structural index.

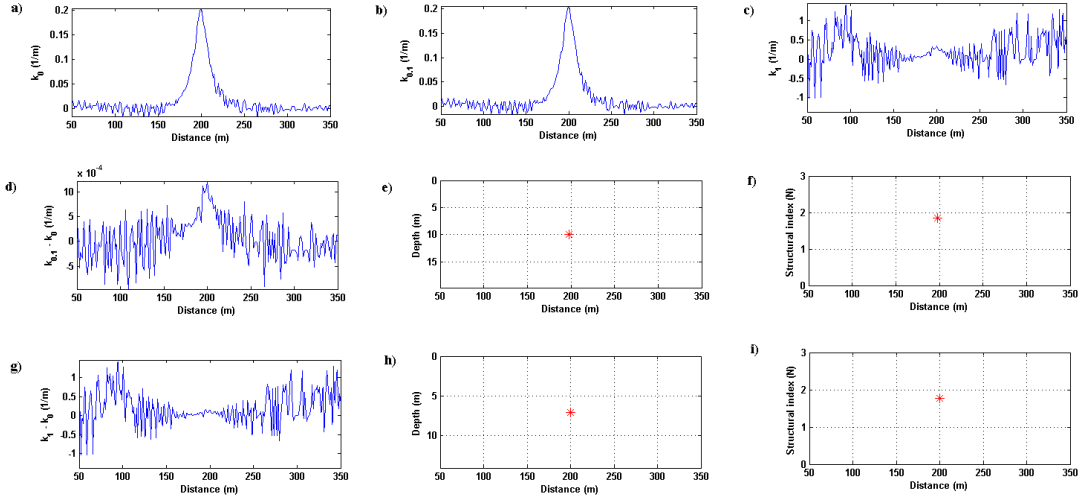


Figure 5.3: Application of the fractional-order local wavenumber to the magnetic field of a horizontal cylinder with addition of noise. a) The 0-order local wavenumber; b) the 0.1-order local wavenumber; c) the 1-order local wavenumber; d) the  $k_{0.1} - k_0$  local wavenumber ; e) the estimated depth from the  $k_{0.1} - k_0$ ; f) the estimated structural index from  $k_{0.1} - k_0$ ; g) the  $k_1 - k_0$  local wavenumber; h) the estimated depth from the  $k_1 - k_0$  and i) the estimated structural index from  $k_1 - k_0$ .

## 5.4 Field Examples

### 5.4.1 A magnetic anomaly from the Pima copper mine, Arizona, USA:

We applied the proposed method to the vertical component magnetic anomaly from the Pima copper mine, Arizona, USA. This anomaly is caused by a thin dike located at a 64 m depth, as known from drilling information (Gay 1963). The profile was digitized with a 10 m step (Figure 5.4a).

We computed the  $k_0$ ,  $k_1$  and  $k_{0.1}$  local wavenumbers (Figures 5.4b,c and e). Then we used the integrer-order difference  $k_1 - k_0$  (Figure 5.4d) to estimate the depth and structural index. The results are 39.9 m and 0.84, respectively (Figure 5.4g and h). Whereas, when using the fractional-order difference  $k_{0.1} - k_0$  (Figure 5.4f), we obtain a 67.88 m as estimated depth and a

1.01 as estimated structural index (Figure 5.4i and j). These results agree well with the known information about the causative source.

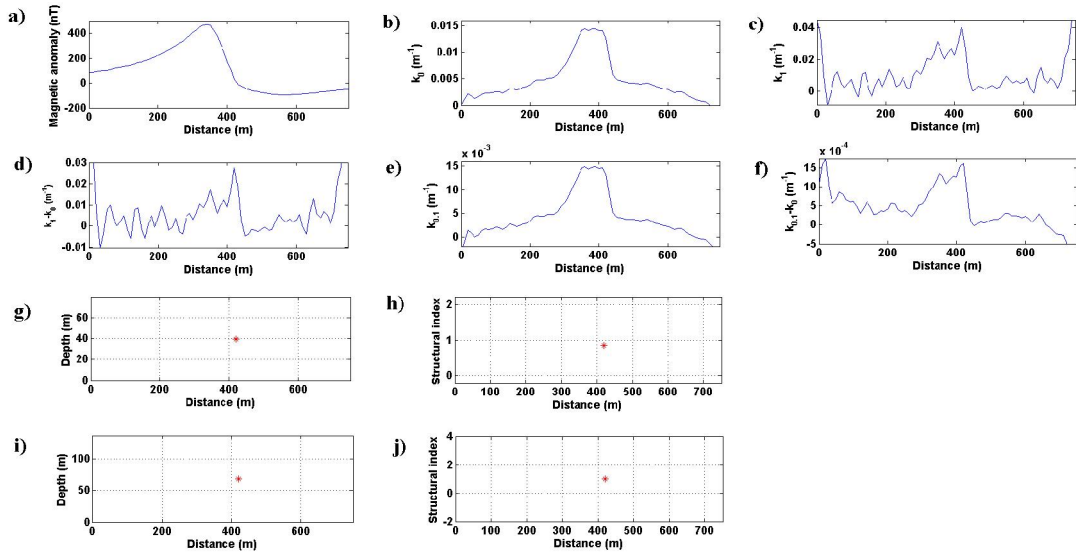


Figure 5.4: Application of the fractional-order local wavenumber to the magnetic anomaly (vertical component) from the Pima copper mine, Arizona, USA. a) The magnetic anomaly profile; b) the 0-order local wavenumber  $k_0$ ; c) the 1-order local wavenumber  $k_1$ ; d) the  $k_I-k_0$  local wavenumber ; e) the 0.1-order local wavenumber  $k_{0.1}$ ; f) the  $k_{0.1}-k_0$  local wavenumber; g) the 39.9 m estimated depth from  $k_I-k_0$ ; f) the estimated structural index  $N=0.84$  from  $k_I-k_0$ ; i) the 67.88 m estimated depth from  $k_{0.1}-k_0$ ; and j) the estimated structural index  $N=1.01$  from  $k_{0.1}-k_0$ .

#### 5.4.2 Magnetic vertical gradient profile from Terina, Catanzaro, Southern Italy:

We applied the fractal-order local wavenumber to a data profile from a magnetic gradient survey carried out for the detection and characterization of archaeological structures at Terina (Catanzaro, Southern Italy) (Figure 5.5a). The sensor is at 2 m height and the measurements were taken with a 0.5 horizontal step. After excavation, a layer of stones and bricks is found at about 0.5 m depth from the surface; i.e., 2.5 m from the sensor (Cella et al., 2015).

We used the 1.8- and 2-order local wavenumbers (Figure 5.5b & c) to estimate the depth. We note that the peaks in  $k_{1.8}$  and  $k_2$  are very correlated and that the use of fractional-order differentiation preserve the shape the form of the peaks allowing a better computation of the difference  $k_2 - k_{1.8}$ , as shown in Figure 5.4d.

We discard depth solutions with structural indices less than -0.2 or more than 2.2. The estimated depths (from the sensor) over the excavated area are 2.5 m and 2.4 m, at horizontal locations  $x=\{10$  and  $12\}$  m respectively (Figure 5.5e). The depth estimates agree well with the excavation findings (Cella et al., 2015). On the other side, at horizontal position  $x=\{16.5$  and  $18\}$  m, the estimated depths are 2.6 m and 2.37 m, respectively. Finally, at  $x= 20$  m, the estimated depth is 4.6 m.

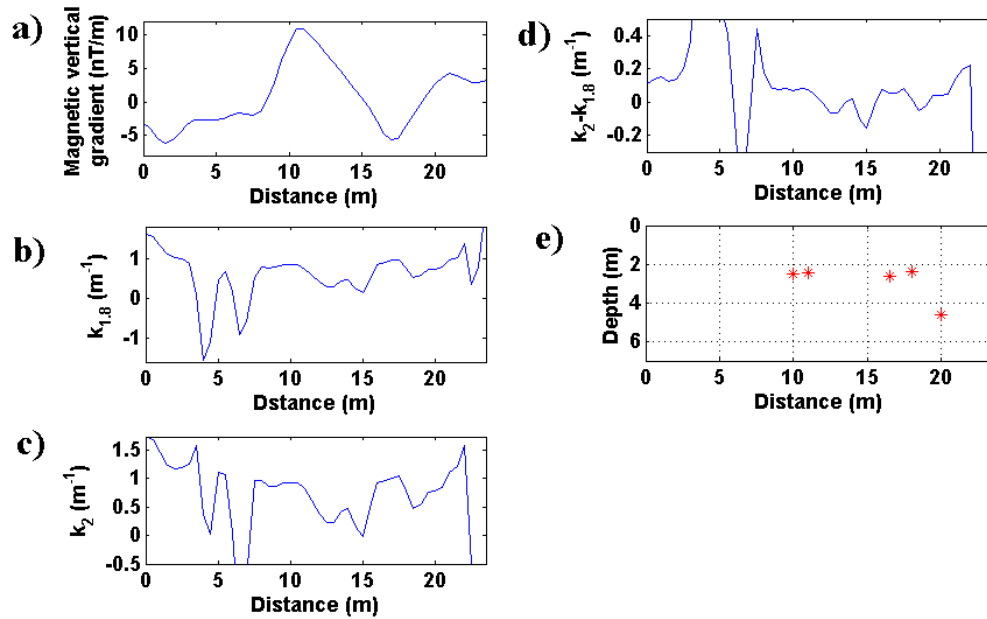


Figure 5.5: Application of the fractional-order local wavenumber to the magnetic vertical gradient anomaly of Terina (Southern Italy). a) The vertical gradient anomaly profile; b) the 1.8-order local wavenumber; c) the 2-order local wavenumber; d) the  $k_2 - k_{1.8}$  local wavenumber ; and e) the estimated depth.

## *Conclusions*

We have introduced the theory of the DEXP method for the interpretation of self-potential data related to oxidation-reduction process and to ground water flow. The method yields estimates of the source horizontal location, depth, and geometry. Also, the method provides information about the type of depth (to the centre, to the top). The DEXP theory yields a number of tools to evaluate the source parameters:

- the depth to the source may be estimated by using the geometric method,
- the symmetry of the whole ridge set can be diagnostic for determining the dip of the dipole moment,
- the scaling function may be used to evaluate the structural index and the depth from any single ridge related to the source, and
- the DEXP transformation may be used to obtain an image of the source distribution and, by searching for its extreme points, to locate at these points the depth and the horizontal position of the source.

The major features of the DEXP method are that no a priori assumptions about the kind of the source are needed; the transformation is very stable; it may be safely used at high-resolution, i.e. using high-order derivatives of the field because of this stability; it is fast and numerically easy to implement for both 2D and 3D problems. The Application of the method to synthetic and real cases in the case of mineral exploration and environmental studies (depth to the water table and sinkhole detection) yields consistent results with the known information about the sources.

We developed a new form of the DEXP imaging method that is fully automatic and independent from the structural index. These properties are derived from applying the DEXP transformation to the ratio between any pair of different-order vertical derivatives of the field or to the partial derivatives of this ratio. Comparing this method to previous imaging methods

(Cribb, 1976; Pedersen, 1991; Patella, 1997; Zhdanov, 2002; and Fedi, 2007), we note that our method is the only one able to giving correct depth and structural index estimation in case of a field generated by a set of different types of sources, such as for instance spherical, cylindrical or fault source distributions. For instance, migration assumes intrinsically a single type of scaling-law and so gives either correct or incorrect depth estimates, depending on the type of source involved (Fedi and Pilkington, 2012); DEXP of potential fields yields correct source estimates if the right scaling-law is assumed, but the multi-source case cannot be accounted in a single step of imaging. In practice, they are both automatic methods, but may fail in a multi-source case. Instead, our new procedure of applying the DEXP transformation not to the potential field itself, but to the ratio of different order vertical derivatives of the field, yields simultaneously correct estimations for each different source in the same image.

This automatic version of the DEXP transformation is fast and warrants accurate depth estimation also for large datasets. It allows also estimation of the structural index. Due to the stability vs. noise of the DEXP transformation we may use high-order derivatives of the field in the ratio and we showed how this feature is useful to circumvent nonlinear effects due to nearby anomalies. We also showed that this feature is in turn useful for establishing whether we are meeting the condition of the field to be homogeneous, and that this issue may be simply assessed by exploring the behaviour of the intercept of the scaling function computed on a selected ridge.

Even if the method is stable vs. noise, another kind of stabilization, however, may be needed because the ratio possibly tends to be singular, and a specific algorithm was adopted to overcome this instability. The application of the method to synthetic and real data shows a good agreement with the known information about the causative sources.

We presented a new automatic method based on the DEXP transformation of the local wavenumber of any order. Our approach consists in analyzing the LWN in the multiscale

context of the DEXP transformation, where a very simple scaling-law occurs for this function, having a fixed form, independent on the kind of source. We have two main advantages compared to other methods using the LWN: a) thanks to the stability property of the DEXP transformation it may be applied to LWN of high-order so that the major factor limiting the applicability of LWN is strongly attenuated; b) the method is fully automatic, so that it may be implemented as a very fast imaging method, mapping every source even of different kind (i.e., characterized by a different structural index) at the correct depth.

With respect to the DEXP transformation of potential fields, our method has instead either advantages or disadvantages: a) the DEXP transformation of the local wavenumber is fully automatic, differently from that of potential field which depends on the structural index; b) the local wavenumber is a nonlinear function of the potential field anomalies of isolated sources and nonlinear effects are likely to occur in complex cases (e.g., Keating, 2009). So, also our DEXP imaging shows non-linear effects, which appear as intense bipolar anomalies (ghosts). However, thanks to this peculiar shape they are easily recognized and excluded from the analysis. In addition, they may be also identified because often they do not correspond to any relevant feature of the measured signal. This is a disadvantage with respect to the DEXP transformation of potential fields, which is instead a linear function with respect to the anomalies of the several sources, and don't present any spurious effect.

The structural index can also be estimated in a fast way, at the extreme points of the DEXP of the local wavenumber. Finally, we remark the high resolution of the method which sharply separates the effect due to the single sources or, in the case of complex non-ideal sources, the contributions due to the several singular parts of the source: this is clearly illustrated in the prism case, where the DEXP transform identifies the sides of the prism. These features make this new automatic method even more attractive.

We show how the local wavenumber method may be improved, providing a new definition in terms of fractional derivatives/integrals. By choosing a suitable fractional order of differentiation/ integration we may keep the noise enhancement to a minimum, so making the LWN method more stable than with the standard approach, based on integer-order field differentiation.

In addition, the use of fractional derivatives/integrals almost tends to preserve the shape of the local wavenumber of different orders: in other words, it does not change the location of the peaks of the local wavenumber allowing a more simple and safe computation of depth and structural index. The method is tested for synthetic and real examples and showed good results compared to the standard local wavenumber method. In this work the fractional-order LWN is applied to the iSPI<sup>TM</sup> method and the LWN-DEXP method, but it can be extended to all the other methods based on the local wavenumber.

## Appendix A

### Division by zero problem in the automatic DEXP method.

Since we are dealing with a ratio between two different orders of derivatives, division by zero or by a very small number may affect the numerical estimate and, consequently, the automatic DEXP method.

Division by zero is a typical problem in data processing and can be treated like that in the imaging of seismic data, occurring for the ratio between the up-going and the down-going wave fields (see e.g., Schleicher et al., 2008). Based on this approach we can check the value of the denominator of  $\mathcal{R}_{mn}$  and increase it by a small amount  $\varepsilon$  ( $0 < \varepsilon < 1$ ) taken as a fraction of the maximum of  $f_n$  at the current depth level. In practice, the ratio,  $\mathcal{R}_{mn}$ , is rewritten as:

$$\mathcal{R}_{mn} = \begin{cases} \frac{f_m}{f_n} & \text{if } f_n \geq \varepsilon \\ \frac{f_m}{\varepsilon} & \text{if } f_n < \varepsilon \end{cases} \quad (\text{A1})$$

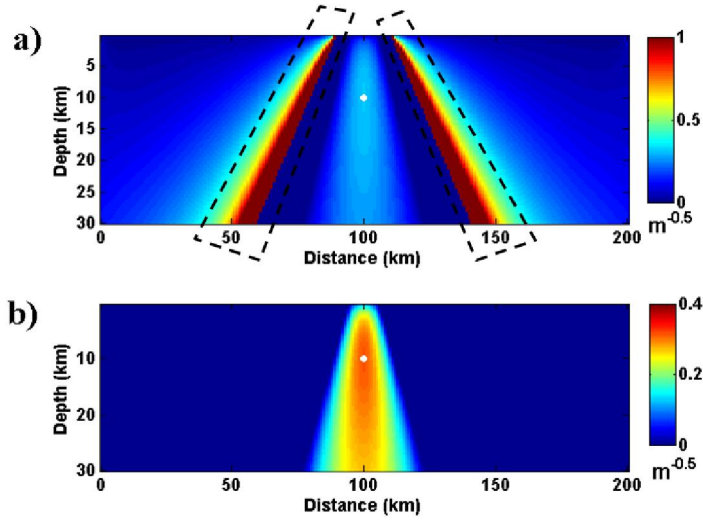


Figure A1: Stabilization of Automatic DEXP. a) The DEXP image of the  $\mathcal{R}_{21}$  without stabilization. The dashed polygons indicate the area affected by the zero-division problem; b) the DEXP image of the ratio  $\mathcal{R}_{21}$  with  $\varepsilon=10\%$  stabilization.

To show how this stabilization process works, let us consider the DEXP transformation ratio of the ratio  $\mathcal{R}_{21}$ , based on the values of the gravity field of an infinite horizontal line source. We note immediately the instability due to the division by near-zero values (Figure A1(a), dashed polygons), as zones characterized by a stripy zone of highs and lows. Even though the maximum of the DEXP is exactly placed at the source position (white dot), there is however need for a more stable DEXP image. Hence, we can use the stabilization approach of equation (A1) to remove the instability zones and so obtain a pretty stabilized image (Figure A1(b)).

## *Appendix B*

### **The homogeneity-degree of the ratio of potential fields of different orders and the ridge behaviour.**

The ratio between two different-order vertical derivatives or two analytic signal moduli of the field is a homogenous function of the spatial coordinates, far away from the zeros of the denominator, with a homogeneity degree equal to half of the difference between their orders. Considering equation (3-6), let us change the origin by a guess value  $\dot{z}_0$ . Both the altitude and the depth will be shifted as  $z - \dot{z}_0$  and  $z_0 - \dot{z}_0$ , respectively. By putting  $z=1/q$ , equation (3-6) becomes:

$$\tau_p(q, \dot{z}_0) = -\frac{(m-n)(1-\dot{z}_0q)}{1-z_0q} \quad (\text{B1})$$

According to the DEXP theory, the scaling function may be effectively used to estimate the structural index (Fedi, 2007; Florio et al., 2009). In fact, it is simple to see in equation (B1) that the slope of  $\tau_p$  becomes a zero-slope straight line when  $\dot{z}_0$  is equal to  $z_0$  and the homogeneity degree is given by the intercept of  $\tau_p$  versus  $q$ . In the case of the ratio  $R$  the intercept is known and equal to  $-(m-n)$ , for homogeneous fields. Hence, from the behaviour of the scaling function (slope and intercept) we can have an idea of how the homogeneity of the field is a good approximation to our dataset. In particular the intercept must be equal to  $-(m-n)$ . Otherwise our assumption will be not verified, at least at the considered set of altitudes. In addition, we can also vary the orders  $m, n$  in such a way to fit the homogeneity condition and so retrieve a valid estimate of  $N$  according to one of the procedures described in the third chapter. If the homogeneity condition is not fully satisfied at a certain set of altitudes, due to the noise and/or the interference effects, we expect also that the ridges will have a curved form contrasting with the straight line occurring for perfect homogeneous fields (Fedi et al., 2009).

## Appendix C

### Numerical evaluation of the $N$ -dependent local-wavenumber equation by Smith et al. (1998) for a fractional order.

We compare the fractional-order local wavenumber, as defined in equation (5-5), with the expression given by Smith et al. (1998) (equation 5-7). This formula, very useful because it depends only on the source parameters ( $N$  and  $z_0$ ), was however demonstrated for an integer order by Smith et al. (1998). So we want to see if it holds also for fractional orders, say  $p=\{1.2, 1.5, 1.8\}$ , by a numerical comparison with the local wavenumber computed through equation (5-5).

We used the magnetic field of three ideal models, a horizontal cylinder, a dike, and a contact at a 10 m depth. As shown in Figure C1, the two expressions of the local wavenumber are comparable and show a perfect matching. This shows that we can use equation (5-7) for the estimation of the depth and structural index with fractional orders.

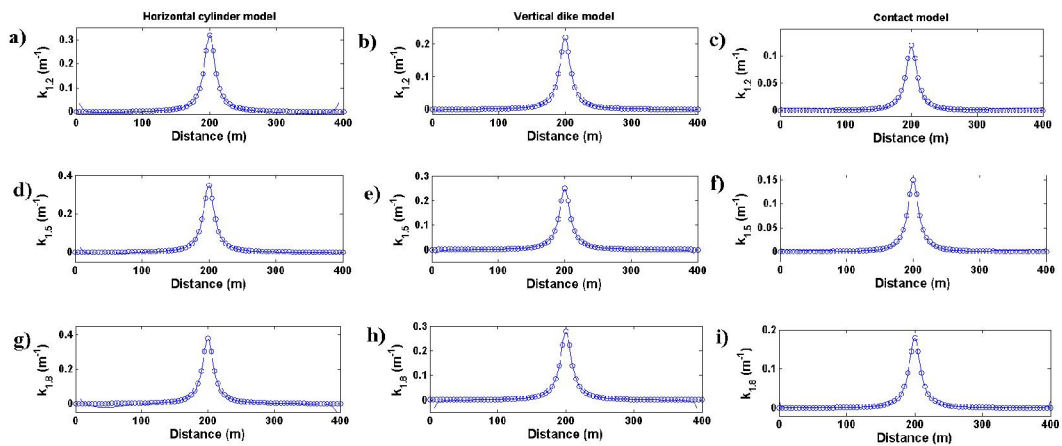


Figure C1: Comparison between the fractional-order local wavenumber  $k_{1.2}$  (a; b; c),  $k_{1.5}$  (d; e),  $k_{1.8}$  (g; h; i), as computed on the basis of equations (5-5) and (5-7), for the magnetic anomaly of a horizontal cylinder, a dike, and a contact. Solid line is for local wavenumber on the basis of equation (5-5); white circles are for local wavenumber based on equation (5-7).

## ***References***

- Abbas, M. A., Fedi, M., and Florio, G., 2014, Improving the local wavenumber method by automatic DEXP transformation. *Journal of Applied Geophysics*, **111**, 250-255.
- Abdelrahman, E., Saber, H., Essa, K., and Fouad, M., 2004, A least-squares approach to depth determination from numerical horizontal self-potential gradients. *Pure and Applied Geophysics*, **161**, 399–411, doi: 10.1007/s00024-003-2446-5.
- Abdelrahman, E.M., and Sharafeldin, S.M., 1997, A least-squares approach to depth determination from residual self-potential anomalies caused by horizontal cylinders and spheres. *Geophysics*, **62**, 44–48, doi: 10.1190/1.1444143.
- Agarwal, B., 1984, Quantitative interpretation of self-potential anomalies. 54th Annual International Meeting, SEG, Expanded Abstracts, 154–157.
- Agarwal, B., and S. Srivastava, 2009, Analyses of self-potential anomalies by conventional and extended Euler deconvolution techniques. *Computers & Geosciences*, **35**, 2231–2238, doi: 10.1016/j.cageo.2009.03.005.
- Aubert, M., Antraygues, P., and Soler, E., 1993, Interpretation des mesures de polarisation spontanée (PS) en hydrogéologie des terrains volcaniques; hypothèse sur l'existence d'écoulements préférentiels sur le flanc du Piton de la Fournaise (Ile de la Reunion). *Bulletin de la Société Géologique de France*, **164**(1), 17-25.
- Aubert, M., and Yéné Atangana, Q., 1996, Self-potential method in hydrogeological exploration of volcanic areas, *Ground Water*, **34**, 1010–1016.
- Aydin, I., 2008, Estimation of the location and depth parameters of 2D magnetic sources using analytical signals. *Journal of Geophysics and Engineering*, **5**, 281–289.

- Babu, H., 2003, Relationship of gravity, magnetic and self-potential anomalies and their application to mineral exploration. *Geophysics*, **68**, 181–184, doi: 10.1190/1.1543205.
- Bansal, A. R., and Dimri, V. P., 2005, Depth determination from nonstationary magnetic profile for scaling geology. *Geophysical Prospecting*, **53**, 399–410, doi: 10.1111/j.1365-2478.2005.00480.x.
- Bansal, A.R., Gabriel, G., and Dimri, V.P., 2010, Power law distribution of susceptibility and density and its relation to seismic properties: An example from the German Continental Deep Drilling Program (KTDB). *Journal of Applied Geophysics*, **72**, 123–128, doi: 10.1016/j.jappgeo.2010.08.001.
- Baranov, V. I., 1975. *Potential fields and their transformations in applied geophysics* (No. 6). Lubrecht & Cramer Limited.
- Bhattacharya, B.B., Biswas, D., Kar, G., and Ghosh, H., 1984, Geoelectric exploration for graphite in the Balangir district, Orissa, India. *Geoexploration*, **22**, 129–143, doi: 10.1016/0016-7142(84)90033-4.
- Bhattacharya, B. B., and Roy, N., 1981, A note on the use of nomograms for self-potential anomalies. *Geophysical Prospecting*, **29**, 102–107, doi: 10.1111/j.1365-2478.1981.tb01013.x.
- Bhattacharya, B. B., Shalivahan, A., Jardani, A., and Bera, A., 2007, Three dimensional probability tomography of self-potential anomalies of graphite and sulphide mineralization in Orissa and Rajasthan, India. *Near Surface Geophysics*, **5**, 223–230, doi: 10.3997/1873-0604.2007004.
- Bogoslovsky, V.V. and Ogilvy, A.A., 1973, Deformations of natural electric fields near drainage structures. *Geophysical Prospecting*, **21**, 716–723.

Bracewell, R., 1965. *The Fourier transform and its applications*. McGraw-Hill Book Co.

Cardarelli, E., Cercato, M., De Donno, G., and Di Filippo, G., 2014, Detection and imaging of piping sinkholes by integrated geophysical methods. *Near Surface Geophysics*, **12**(3), 439-450.

Cella, F., Fedi, M., and Florio, G., 2009, Toward a full multiscale approach to interpret potential fields. *Geophysical Prospecting*, **57**, 543–557, doi: 10.1111/j.1365-2478.2009.00808.x.

Cella F., Paoletti V., Florio G., and Fedi M., 2015, Characterizing Elements of Urban Planning in Magna Graecia Using Geophysical Techniques: the Case of Tirenna (Southern Italy). *Archaeological Prospection*, doi: 10.1002/arp.1507.

Centamore, E., Nisio, S. and Rossi, D., 2009, The San Vittorino Sinkhole Plain: relationships between bedrock structure, sinking processes, seismic events and hydrothermal springs. *Italian Journal of Geoscience*, **128**(3), 629–639.

Cooper, G.R.J., and Cowan, D.R., 2003, The application of fractional calculus to potential field data. *Exploration Geophysics*, **34** (4), 51–56.

Cordell, L. And Grauch, V.J.S., 1985, Mapping basement magnetization zones from aeromagnetic data in the San Juan basin, New Mexico, in *The Utility of Regional Gravity and Magnetic Anomaly Maps*, pp. 181–197, ed. Hinze, W.J., Society of Exploration Geophysicists.

Cribb, J., 1976, Application of the generalized linear inverse to the inversion of static potential data. *Geophysics*, **41**, 1365–1369.

Darnet, M., Marquis, G., and Sailhac, P., 2003, Estimating aquifer hydraulic properties from the inversion of surface Streaming Potential (SP) anomalies. *Geophysical Research Letters*, **30**(13), 1679, doi:10.1029/2003GL017631.

Dobrin, M. B., 1960. *Introduction to geophysical prospecting*: McGraw-Hill.

Fedi, M., 2003, Global and local multiscale analysis of magnetic susceptibility data. *Pure and Applied Geophysics*, **160**, 2399–2417, doi: 10.1007/s00024-003-2401-5.

Fedi, M., 2007, DEXP: A fast method to determine the depth and the structural index of potential fields sources. *Geophysics*, **72**(1), I1–I11, doi: 10.1190/1.2399452.

Fedi, M., and Abbas, M. A., 2013, A fast interpretation of self-potential data using the depth from extreme points method. *Geophysics*, **78**(2), E107-E116.

Fedi, M., and Cascone, L., 2011, Composite continuous wavelet transform of potential fields with different choices of analyzing wavelets. *Journal of Geophysical Research*, **116**, B07104, doi: 10.1029/2010JB007882.

Fedi, M., Cella, F., Quarta, T., and Villani, A.V., 2010, 2D Continuous wavelet transform of potential fields due to extended source distributions. *Applied and Computational Harmonic Analysis*, **28**, 320–337, doi: 10.1016/j.acha.2010.03.002.

Fedi, M., and Florio, G., 2006, SCALFUN: 3D analysis of potential field scaling function to determine independently or simultaneously structural index and depth to source. 76th Annual International Meeting, SEG, Expanded Abstracts, 963–967.

Fedi, M.G., Florio, 2013, Determination of the maximum-depth to potential field sources by a maximum structural index method. *Journal of Applied Geophysics*, **88**, 154–160.

- Fedi, M., Florio, G., and Quarta, T., 2009, Multiridge analysis of potential fields: Geometric method and reduced Euler deconvolution. *Geophysics*, **74**(4), L53–L65, doi: 10.1190/1.3142722.
- Fedi, M., and Pilkington, M., 2012, Understanding imaging methods for potential field data. *Geophysics*, **77**(1), G13–G24, doi: 10.1190/geo2011-0078.1.
- Fernández-Martínez, J.L., García-Gonzalo, E., and Naudet, V., 2010, Particle swarm optimization applied to solving and appraising the streaming-potential inverse problem. *Geophysics*, **75**(4), WA3-WA15.
- Florio, G. and Fedi, M., 2014, Multiridge Euler deconvolution. *Geophysical Prospecting*, **62**(2), 333–351.
- Florio, G., Fedi, M., and Rapolla, A., 2009, Interpretation of regional aeromagnetic data by the scaling function method: The case of Southern Apennines (Italy). *Geophysical Prospecting*, **57**, 479–489, doi: 10.1111/j.1365-2478.2009.00807.x.
- Fournier, C., 1989, Spontaneous Potentials and Resistivity Surveys Applied To Hydrogeology In A Volcanic Area: Case History Of The Chaîne Des Puys (Puy-De-Dôme, France). *Geophysical Prospecting*, **37**, 647– 668.
- Gay, P., 1963, Standard curves for interpretation of magnetic anomalies over tabular bodies. *Geophysics*, **28**, 161–200.
- Gerovska, D., Araúzo-Bravo, M.J., Stavrev, P., 2009, Estimating the magnetization direction of sources from southeast Bulgaria through correlation between reduced-to-the-pole and total magnitude anomalies. *Geophysical Prospecting*, **57**, 491–505.

- Gibert, D., and Sailhac, P., 2008, Comment on “Self-potential signals associated with preferential groundwater flow pathways in sinkholes” by A. Jardani, J. P. Dupont, and A. Revil. *Journal of Geophysical Research*, **113**, B03210, doi: 10.1029/2007JB004969.
- Gunn, P.J., 1975, Linear Transformations of Gravity and Magnetic Fields. *Geophysical Prospecting*, **23**, 300–312.
- Gunn, P.J., Fitzgerald, D., Yassi, N., and Dart, P., 1997, New Algorithms for Visually Enhancing Airborne Geophysical Data. *Exploration Geophysics*, **28**, 220–224.
- Heiland, C. A., Tripp, M.R., and Wantland, D., 1945, Geophysical surveys at the Malachite Mine, Jefferson County, Colorado. American Institute of Mining and Metallurgical Engineers, 164, 142–154.
- Hsu, S.K., 2002, Imaging magnetic sources using Euler’s equation. *Geophysical Prospecting*, **50**, 15–25.
- Hsu, S.K., Coppens, D., and Shyu, C.T., 1998, Depth to magnetic source using the generalized analytic signal. *Geophysics*, **63**, 1947–1957.
- Iuliano, T., Mauriello, P., and Patella, D., 2002, Looking inside Mount Vesuvius by potential fields integrated probability tomographies. *Journal of Volcanology and Geothermal Research*, **113**, 363–378, doi: 10.1016/S0377-0273(01)00271-2.
- Jackson, D.B., and Kauahikaua, J., 1987. Regional self-potential anomalies at Kilauea volcano. *USGS Professional paper*, **1350**(40), 947-959.
- Jardani, A., Revil, A., Akoa, F., Schmutz, M., Florsch, N., and Dupont, J. P., 2006, Least squares inversion of self-potential (SP) data and application to the shallow flow of ground

water in sinkholes. *Geophysical Research Letters*, **33**(19), L19306, doi:10.1029/2006GL027458.

Jardani, A., Revil, A., Barrash, W., Crespy, A., Rizzo, E., Straface, S., Cardiff, M., Malama, B., Miller, C., and T. Johnson, 2009, Reconstruction of the Water Table from Self-Potential Data: A Bayesian Approach. *Groundwater*, **47**(2), 213-227.

Jardani, A., Revil, A., Boleve, A., Crespy, A., Dupont, J.P., and Barrash, W., 2007, Tomography of the Darcy velocity from self potential measurements. *Geophysical Research Letters*, **34**, L24403, doi: 10.1029/2007GL031907.

Jardani, A., Revil, A., Bolève, A., and Dupont, J.P., 2008, Three-dimensional inversion of self-potential data used to constrain the pattern of groundwater flow in geothermal fields. *Journal of Geophysical Research*, **113**, B09204, doi: 10.1029/2007JB005302.

Keating, P., 2009, Improved use of the local wavenumber in potential-field interpretation. *Geophysics*, **74**(6), L75–L85.

Li, X., 2006, Understanding 3D analytic signal amplitude. *Geophysics*, **71**(2), L13–L16.

Marchetti, M., Chiappini, M., and Meloni, A., 1998, A test site for the magnetic detection of buried steel drums. *Annals of Geophysics*, **41**(3), 491–498.

Meiser, P., 1962, A method of quantitative interpretation of self potential measurements: *Geophysical Prospecting*, **10**, 203–218, doi: 10.1111/j.1365-2478.1962.tb02009.x.

Mendonça, C., 2008, Forward and inverse self-potential modeling in mineral exploration. *Geophysics*, **73**(2), F33–F43, doi: 10.1190/1.2821191.

Minsley, B., Sogade, J., and Morgan, F., 2007, Three-dimensional source inversion of self-potential data. *Journal of Geophysical Research*, **112**, B02202, doi: 10.1029/2006JB004262.

- Moreau, F., Gibert, D., Holshneider, M., and Saracco, G., 1997, Wavelet analysis of potential fields. *Inverse Problems*, **13**, 165–178, doi: 10.1088/0266-5611/13/1/013.
- Mushayandebvu, M. F., van Driel, P., Reid, A.B., and Fairhead, J.D., 2001, Magnetic source parameters of two-dimensional structures using extended Euler deconvolution. *Geophysics*, **66**, 814–823, doi: 10.1190/1.1444971.
- Nabighian, M.N., 1972, The analytic signal of two-dimensional magnetic bodies with polygonal cross-section: its properties and use for automated anomaly interpretation. *Geophysics*, **37**(3), 507–517.
- Naudet, V., Revil, A., Bottero, J.-Y., and Bégassat, P., 2003, Relationship between self-potential (SP) signals and redox conditions in contaminated groundwater. *Geophysical Research Letters*, **30**, 2091–2094, doi: 10.1029/2003GL018096.
- Naudet, V., Revil, A., Rizzo, E., Bottero, J.-Y., and Bégassat, P., 2004, Groundwater redox conditions and conductivity in a contaminant plume from geoelectrical investigations. *Hydrology and Earth System Sciences*, **8**, 8–22, doi: 10.5194/hess-8-8-2004.
- Patella, D., 1997a, Introduction to ground surface self-potential tomography. *Geophysical Prospecting*, **45**, 653–681, doi: 10.1046/j.1365-2478.1997.430277.x.
- Patella, D., 1997b, Self-potential global tomography including topographic effects. *Geophysical Prospecting*, **45**, 843–863, doi: 10.1046/j.1365-2478.1997.570296.x.
- Paul, M., 1965, Direct interpretation of self-potential anomalies caused by inclined sheets of infinite horizontal extensions. *Geophysics*, **30**, 418–423, doi: 10.1190/1.1439596.
- Pedersen, L.B., 1991, Relations between potential fields and some equivalent sources. *Geophysics*, **56**, 961–971.

- Phillips, J.D., Hansen, R.O., Blakely, R.J., 2007, The use of curvature in potential-field interpretation. *Exploration Geophysics*, **38** (2), 111–119.
- Pilkington, M., and Todoeschuck, J.P., 1993, Fractal magnetization of continental crust. *Geophysical Research Letters*, **20**, 627–630, doi: 10.1029/92GL03009.
- Rao, A.D., Babu, H., and Sivakumar Sinha, G.D., 1982, A Fourier transform method for the interpretation of self-potential anomalies due to two dimensional inclined sheet of finite depth extent. *Pure and Applied Geophysics*, **120**, 365–374, doi: 10.1007/BF00877042.
- Rao, A.D., and Babu, R., 1983, Quantitative interpretation of self-potential anomalies due to two-dimensional sheet-like bodies. *Geophysics*, **48**, 1659–1664, doi: 10.1190/1.1441446.
- Reid, A.B., Allsop, J.M., Granser, H., Millett, A.J. and Somerton, I.W., 1990, Magnetic interpretation in three dimensions using Euler deconvolution. *Geophysics*, **55**, 80–91.
- Revil, A., Ehouarne, L., and Thyreault, E., 2001, Tomography of self-potential anomalies of electrochemical nature. *Geophysical Research Letters*, **28**, 4363–4366, doi: 10.1029/2001GL013631.
- Revil, A., Naudet, V. and Meunier, J.D., 2004,. The hydroelectric problem of porous rocks: Inversion of the water table from self-potential data. *Geophysical Journal International*, **159**, 435–444.
- Revil, A., Naudet, V. , Nouzaret, J. , and Pessel, M., 2003, Principles of electrography applied to self-potential electrokinetic sources and hydrogeological applications. *Water Resources Research*, **39**(5), 1114, doi:10.1029/2001WR000916.

- Rizzo, E., Suski, B., Revil, A., Straface, S., and Troisi, S., 2004, Self-potential signals associated with pumping-tests experiments. *Journal of Geophysical Research*, **109**, B10203, doi: 10.1029/2004JB003049.
- Roest, W.R., Verhoef, J. and Pilkington, M., 1992, Magnetic interpretation using the 3-D analytic signal. *Geophysics*, **57**(1), 116–125.
- Roy, L., 2001, Short note: Source geometry identification by simultaneous use of structural index and shape factor. *Geophysical Prospecting*, **49**, 159–164, doi: 10.1046/j.1365-2478.2001.00239.x.
- Sailhac, P., and Marquis, G., 2001, Analytic potentials for the forward and inverse modeling of SP anomalies caused by subsurface fluid flow. *Geophysical Research Letters*, **28**, 1851–1854, doi: 10.1029/2000GL012457.
- Salem, A., 2011, Multi-deconvolution analysis of potential field data. *Journal of applied Geophysics*, **74**, 151–156.
- Salem, A., and Ravat, D., 2003, A combined analytic signal and Euler method (AN-EUL) for automatic interpretation of magnetic data. *Geophysics*, **68**, 1952–1961.
- Salem, A., Ravat, D., Gamey, T.J. and Ushijima, K., 2002, Analytic signal approach and its applicability in environmental magnetic investigations, *Journal of Applied Geophysics*, **49**, 231–244.
- Salem, A., Ravat, D., Smith, R., and Ushijima, K., 2005, Interpretation of magnetic data using an enhanced local wavenumber (ELW) method. *Geophysics*, **70**(1), L7–L12, doi: 10.1190/1.1884828.

- Salem, A., Williams, S., Fairhead, D., Smith, R., Ravat, D., 2008, Interpretation of magnetic data using tilt-angle derivatives. *Geophysics*, **73** (1), L1–L10.
- Sato, M., and Mooney, H., 1960, The electrochemical mechanism of sulfide self-potentials. *Geophysics*, **25**, 226–249, doi: 10.1190/1.1438689.
- Schleicher, J., Costa, J.C. and Novais, A., 2008, A comparison of imaging conditions for wave-equation short-profile migration. *Geophysics*, **73**, S219–S227.
- Shi, W., and Morgan, F. D., 1996, Non-uniqueness in self-potential inversion. 66th Annual International Meeting, SEG, Expanded Abstracts, 950–953.
- Smith, R.S., Thurston, J.B., Dai, T.-F. & McLeod, I.N., 1998, ISPI<sup>TM</sup> – the improved source parameter imaging method. *Geophysical Prospecting*, **46**(2), 141–152.
- Srivastava, S., and Agarwal, B., 2009, Interpretation of self-potential anomalies by enhanced local wavenumber technique. *Journal of Applied Geophysics*, **68**, 259–268, doi: 10.1016/j.jappgeo.2008.11.011.
- Stavrev, P., Gerovska, D., Araúzo-Bravo, M.J., 2009, Depth and shape estimates from simultaneous inversion of magnetic fields and their gradient components using differential similarity transforms. *Geophysical Prospecting*, **57**, 707–717.
- Thompson, D. T., 1982, EULDPH: A new technique for making computer assisted depth estimates from magnetic data. *Geophysics*, **47**, 31–37, doi: 10.1190/1.1441278.
- Thurston, J.B. and Smith, R.S., 1997, Automatic conversion of magnetic data to depth, dip, and susceptibility contrast using the SPI<sup>TM</sup> methods, *Geophysics*, **62**(3), 807–813.

Trique, M., Perrier, F., Froidefond, T., Avouac, J.P., and Hautot, S., 2002, Fluid flow near reservoir lakes inferred from the spatial and temporal analysis of the electric potential. *Journal of Geophysical Research*, **107**, 2239–2266, doi: 10.1029/2001JB000482.

Yüngül, S., 1950, Interpretation of spontaneous polarization anomalies caused by spherical ore bodies. *Geophysics*, **15**, 237–246, doi: 10.1190/1.1437597.

Vallée, M.A., Keating, P., Smith, R.S. and St-Hilaire, C., 2004, Estimating depth and model type using the continuous wavelet transform of magnetic data. *Geophysics*, **69**, 191–199.

Zablocki, C. J., 1978, Streaming potentials resulting from the descent of meteoric water. A possible source mechanism for Kilauean self-potential anomalies. *Trans. Geotherm. Resour. Council*, **2**, 747-748.

Zhdanov, M.S., 2002, *Geophysical Inverse Theory and Regularization Problems*. Elsevier Science.

## *Acknowledgements*

I would like to give my sincere thanks to my supervisor, Prof. Maurizio Fedi, who accepted me as PhD student without any hesitation. Thereafter, he offered me so much advice, patiently supervised me, and always guided me in the right direction. I have learned a lot from him, without his help I could not have finished my thesis. Also, I thank Prof. Giovanni Florio, for his very useful advices and discussions.

Special thanks are also given to Dr. Ed. K. Biegert, Shell International Exploration and Production, Inc., for reviewing this dissertation and for his valuable comments. Also, I would like to thank Prof. Ettore Cardarelli, University of Rome “La Sapienza”, for giving me the SP data of the area of San Vittorino Plain, and to Prof. Federico Cella, University of Calabria, and Dr. Valeria Paoletti, University of Naples “Federico II” for giving me the magnetic data profile of Terina archaeological site.

Last but not least I thank my friends Davide, Simone, Gabriella, Daniela, Raffaele, Mauro, Domenico, Mahak Singh and Maurizio who shared these years with me, supporting me and filling my days with joy.